

Copyright Warning & Restrictions

The copyright law of the United States (Title 17, United States Code) governs the making of photocopies or other reproductions of copyrighted material.

Under certain conditions specified in the law, libraries and archives are authorized to furnish a photocopy or other reproduction. One of these specified conditions is that the photocopy or reproduction is not to be “used for any purpose other than private study, scholarship, or research.” If a user makes a request for, or later uses, a photocopy or reproduction for purposes in excess of “fair use” that user may be liable for copyright infringement,

This institution reserves the right to refuse to accept a copying order if, in its judgment, fulfillment of the order would involve violation of copyright law.

Please Note: The author retains the copyright while the New Jersey Institute of Technology reserves the right to distribute this thesis or dissertation

Printing note: If you do not wish to print this page, then select “Pages from: first page # to: last page #” on the print dialog screen

The Van Houten library has removed some of the personal information and all signatures from the approval page and biographical sketches of theses and dissertations in order to protect the identity of NJIT graduates and faculty.

ABSTRACT

**ASSEMBLY AND DETECTION OF 3-D QR CODES
THROUGH ADDITIVE MANUFACTURING AND TERAHERTZ IMAGING**

by
Patrick Dunn

Automatic identification and data capture, or AIDC, plays a substantial role in contemporary business, advertising, and military needs. The purpose of this study is to generate a potential alternative to current AIDC approaches by constructing three-dimensional plastic tags (or '3D QR codes') using additive manufacturing techniques and interrogate them using Terahertz radiation. 3D Quick Response (QR) codes are designed in 3D computer-aided design software. The QR codes are 3D structures embedded in the printed plastic in which an air gap in the plastic (or an air gap filled in with another type of plastic) indicates a bit of information. Information is encoded into the structure via the absence or presence of an air gap as well as its physical distance from the front surface of the plastic. The QR codes are fabricated using a fusion deposition modeling (FDM) 3D printer. The embedded information in the QR code is read out using time-domain Terahertz (THz) electromagnetic pulses.

**ASSEMBLY AND DETECTION OF 3-D QR CODES
THROUGH ADDITIVE MANUFACTURING AND TERAHERTZ IMAGING**

**by
Patrick Dunn**

**A Thesis
Submitted to the Faculty of
New Jersey Institute of Technology
and Rutgers State University New Jersey- Newark
in Partial Fulfillment of the Requirements for the Degree of
Master of Science in Applied Physics**

Federated Department of Physics

May 2021

APPROVAL PAGE

**ASSEMBLY AND DETECTION OF 3-D QR CODES
THROUGH ADDITIVE MANUFACTURING AND TERAHERTZ IMAGING**

Patrick Dunn

Dr. John F. Federici, Thesis Advisor Distinguished Professor of Physics, NJIT	Date
--	------

Dr. Ian Gatley, Committee Member Distinguished Professor of Physics, NJIT	Date
--	------

Dr. Benjamin Thomas, Committee Member Assistant Professor of Physics, NJIT	Date
---	------

BIOGRAPHICAL SKETCH

Author: Patrick Dunn
Degree: Master of Science
Date: May 2021

Undergraduate and Graduate Education:

- Master of Science in Applied Physics
New Jersey Institute of Technology, Newark, NJ, 2021
- Bachelor of Science in Physics,
The College of New Jersey, Ewing, NJ, 2016

Major: Applied Physics

Dedicated to those who have inspired me - Mom, Dad, Steph, Rena, Dr. Smock,
and Kairi

ACKNOWLEDGMENT

I would like to express gratitude to my advisor, Dr. John Federici, for his guidance and support through the research and composition process. I would like to thank my committee members, Dr. Ian Gatley and Dr. Benjamin Thomas, for their valuable insights.

I would like to thank the members of the NJIT Additive Manufacturing Lab who have helped me along the way: Sam Gatley, Nicholas Warholak, Jessy Nemati, and Alexander Clark. In addition, I would like to give a special acknowledgement to Louis Rizzo, without whom I may not have been able to overcome many of the difficulties in my research.

TABLE OF CONTENTS

Chapter	Page
1 INTRODUCTION.....	1
1.1 Background Information.....	1
1.2 Objective.....	2
2 RELATED RESEARCH.....	4
2.1 Terahertz Tags.....	4
2.2 Fabrication Methods.....	7
2.3 Deconvolution.....	8
3 RELEVANT TECHNOLOGIES.....	10
3.1 Terahertz Time-Domain Spectroscopy.....	10
3.2 3D Printing	14
3.3 Deconvolution Processing.....	15
4 OPTICAL THEORY.....	18
4.1 Refractive Indices.....	18
4.2 Waveform Analysis.....	22
5 3D TERAHERTZ QR CODE.....	25
5.1 Design.....	25
5.2 Data Collection.....	29
5.3 Uncovered QR Code.....	35
5.4 Clandestine QR Code.....	39
6 ANALYSIS.....	45
6.1 Decoding Algorithm.....	45

TABLE OF CONTENTS (Continued)

Chapter	Page
6.2 QR Code Simulator.....	50
7 CONCLUSION.....	57
7.1 Results.....	57
7.2 Future Research/Applications.....	58
APPENDIX A IMPORT FUNCTION.....	60
APPENDIX B DECODING ALGORITHM.....	61
APPENDIX C QR CODE SIMULATOR.....	63
C.1 Example of parameters defined in EXCEL file used in producing simulated 3D QR codes.....	63
C.2 QR Code Simulator Main Program.....	63
REFERENCES.....	66

LIST OF TABLES

Table	Page
3.1 Printing and Material Parameters of Common 3D Printed Materials at 500GHz..	19

LIST OF FIGURES

Figure	Page
2.1 An example of a Matrix InfraStruct prototype design.....	5
2.2 Prototype designs for InfraStruct tags including (a) Gray code, (b) geometric, (c) random void, (d) matrix, and (e) visual designs.....	5
2.3 A terahertz tag composed of two Bragg mirrors and a central defect.....	6
2.4 THz frequency-wavelet deconvolution result for a typical THz waveform.....	9
3.1 The main component of a Terahertz pulse generation device.....	10
3.2 A THz imaging device interacting with a sample layered object.....	11
3.3 An example of a waveform recorded by the Terahertz control unit.....	12
3.4 Pump-probe layout for different lengths of the probe beam.....	13
3.5 Fourier transform of a THz waveform mapped to a logarithmic scale.....	14
3.6 An example of a raw waveform from a 3D QR code pixel and its deconvolved counterpart.....	17
4.1 An example of a THz pulse interacting with a sample tag.....	23
5.1 Uncovered 3D QR code as seen in CAD Software.....	27
5.2 Clandestine 3D QR code as seen in CAD software.....	28
5.3 A sample 3D QR tag mounted in front of THz imaging device.....	30
5.4 An example of the script for a recipe on the T-Ray 5000 and the time-domain and frequency-domain filtering applied.....	33
5.5 An example of an image taken of a 3D QR code tag in the .5-2 THz range.....	34
5.6 An example of a '01' pixel for the uncovered tag as a deconvolved waveform...	36
5.7 An example of a '10' pixel for the uncovered tag as a deconvolved waveform...	37
5.8 An example of a '11' pixel for the uncovered tag as a deconvolved waveform...	38

LIST OF FIGURES (Continued)

Figure	Page
5.9 An example of a ‘00’ pixel for the uncovered tag as a deconvolved waveform...	39
5.10 An example of a ‘01’ pixel for the clandestine tag as a deconvolved waveform...	41
5.11 An example of a ‘11’ pixel for the clandestine tag as a deconvolved waveform...	42
5.12 An example of a ‘10’ pixel for the clandestine tag as a deconvolved waveform...	43
5.13 An example of a ‘00’ pixel for the uncovered tag as a deconvolved waveform...	44
6.1 Time intervals and binary designation on ‘01’ deconvolved waveform.....	47
6.2 Time intervals and binary designation on ‘11’ deconvolved waveform.....	48
6.3 Time intervals and binary designation on ‘10’ deconvolved waveform.....	48
6.4 Time intervals and binary designation on ‘00’ deconvolved waveform.....	49
6.5 A typical raw and deconvolved waveform created by the QR code simulator.....	51
6.6 A deconvolved simulated ‘10’ pixel for a four-layer structure.....	52
6.7 Example of simulated QR code attenuated to decoding limit.....	54
6.8 Example of simulated QR code with thin layers leading to waveform overlap viewed with a wide and narrow time axis.....	56

CHAPTER 1

INTRODUCTION

1.1 Background Information

The ability to identify and collect data about an object easily through tagging methods has made significant progress since its first major implementation in the 1970s [Yang & Fathy 2005]. Automatic Identification and Data Capture, or AIDC, plays a substantial role in contemporary business, advertising, and military needs. While the current technologies of barcodes, Quick Response (QR) codes, and Radio Frequency Identification (RFID) tags can fulfill these purposes, rising concerns of security and functionality call for a novel approach to AIDC. One attractive option comes in the intersection of two rising technologies: additive manufacturing and Terahertz (THz) imaging. The purpose of this study is to generate a potential alternative to current AIDC approaches by constructing three-dimensional plastic tags (or ‘3D QR codes’) using additive manufacturing techniques and collecting data from them using Terahertz radiation.

While current tagging methods used in industry are extremely useful, they also have numerous disadvantages. Conventional barcodes and QR codes face a major drawback in that they require a direct line of sight between the detector and code, meaning that the code must be on the outside of the object in an accessible position. These codes can easily be damaged or obstructed which can lead to failure in detection, especially since they must be featured on the exterior of the object. Another major concern is that, since the codes cannot be hidden, they are available to anyone who can

see it, which can lead to illegitimate counterfeiting of consumer product details, or access to information intended to be private [Kato & Tan 2007]. Finally, barcodes/QR codes can be considered unsightly, which is a weakness in the design of consumer products.

Radio-frequency identification systems answer some of the shortcomings of conventional codes, but also have characteristics that can be problematic. RFID readers will typically detect all tags in a certain proximity, making it difficult to isolate objects without using barriers to block the emitted radio waves [Subramanian et al 2005]. While RFID tags come in passive and active varieties, passive tags can only store minimal amounts of information, and active tags can be considerably expensive. ‘Chipless’ RFIDs offer a nice middle ground, but must be constructed fairly large, as they operate in the gigahertz range [Bernier et al. 2011]. Security concerns also plague RFID tags, as their relative popularity have led to many instances of unauthorized access to data, necessitating a constant update in RFID encryption technology.

1.2 Objective

Applications of additive manufacturing and THz imaging offer a unique remedy to many of the mentioned issues. Individualized tags can be digitally fabricated easily and for relatively inexpensively through 3D printing. The tags can potentially be printed as part of the object (and enclosed inside of it) if the object is made of plastic or some other compatible material, such as ceramics [Willis & Wilson 2003].

The Terahertz gap of the electromagnetic spectrum exists between the microwave and far-infrared frequencies, and is on the order of 10^{12} Hz. Radiation in the THz range can easily penetrate a variety of materials, including commonly used plastics and

ceramics. THz radiation will not penetrate through aqueous or metallic material. While X-rays can also enter these materials, THz radiation is non-ionizing, making it much safer for the implementation offered by this thesis. THz waves also require a smaller power emission than X-rays in general [Willis & Wilson 2003]. As it stands currently, Terahertz technology is not as ubiquitous as that in other electromagnetic ranges. This provides an inherent layer of security, as THz imaging devices are relatively scarce, and thus tags read by them are less accessible (though this can of course change in the future) [Bernier et al. 2011]. A notable use of this new type of tag could be for clandestine tagging of military inventory, as it does not require direct line of sight, electronic components, or oversized construction.

The objective of this study was to construct a prototype of such a 3D printed tag (or 3D QR code), and to measure it using THz time-domain spectroscopy. Using the on-board Terahertz control unit (TCU) analysis software and MATLAB software, a unique code can be outputted associated with the internal geometry and materials within the tag.

CHAPTER 2

RELATED RESEARCH

2.1 Terahertz Tags

A related study that has helped to inspire this research was conducted by K.D.D Willis and A.D. Wilson. The study features five prototype designs for encoded information tags that were analyzed using time-domain spectroscopy in the Terahertz region. The tags were constructed using either additive or subtractive manufacturing techniques, depending on the design.

One of the designs featured, which they call the ‘Matrix InfraStruct,’ is the basis of the design utilized in this thesis, with a few major key differences discussed later on. Their design features three polystyrene slides, each with a 3x3 grid of ‘bits’ represented by either an air gap (formed with laser cutting) or with the plastic not removed. The three slides are layered on top of each other in an ABS case, creating a grid of 27 bits (3x3x3) which are measured in reflection, with the air gap representing a binary ‘0’, and the filled-in polystyrene representing a ‘1’. This design is illustrated in Figure 2.1.

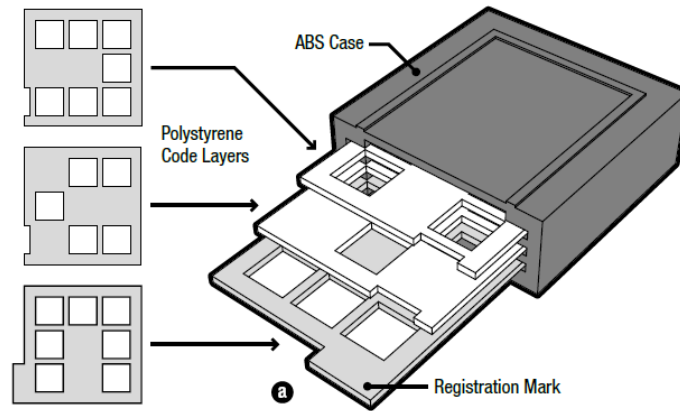


Figure 2.1 An example of a Matrix InfraStruct prototype design.

Source: Willis, K. D., & Wilson, A. D. (2013). InfraStructs: fabricating information inside physical objects for imaging in the Terahertz region. *ACM Transactions on Graphics (TOG)*, 32(4), 138.

Other designs included: multi-layer gray code patterns detected by ray scan, unique geometric structures read by planar scan, random void patterns read by volumetric scans, and visual watermarks to be imaged volumetrically, but identified by the human eye for anti-counterfeiting. These designs are shown in Figure 2.2. The decoding and analysis for each of these designs affirmed their proof of concept [Willis & Wilson 2013].

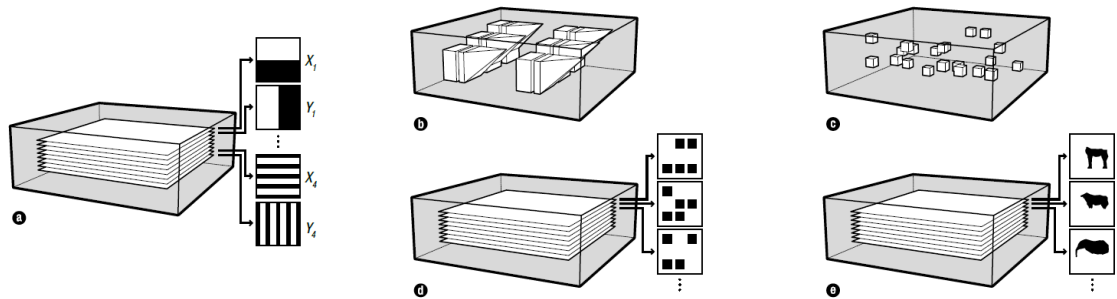


Figure 2.2 Prototype designs for InfraStruct tags including (a) Gray code, (b) geometric, (c) random void, (d) matrix, and (e) visual designs.

Source: Willis, K. D., & Wilson, A. D. (2013). InfraStructs: fabricating information inside physical objects for imaging in the Terahertz region. *ACM Transactions on Graphics (TOG)*, 32(4), 138.

In a study by M. Bernier et al., the authors explore the concept of a chipless tag, similar to current chipless RFIDs, but are encoded for the Terahertz regime. The tag consists of two identical Bragg mirrors separated by a dielectric defect, for which the researchers used silicon and air gaps as their materials. The tag is to be read in 1-dimensional transmission, with the information being coded with the presence or absence of resonance peaks within the Bragg mirrors.

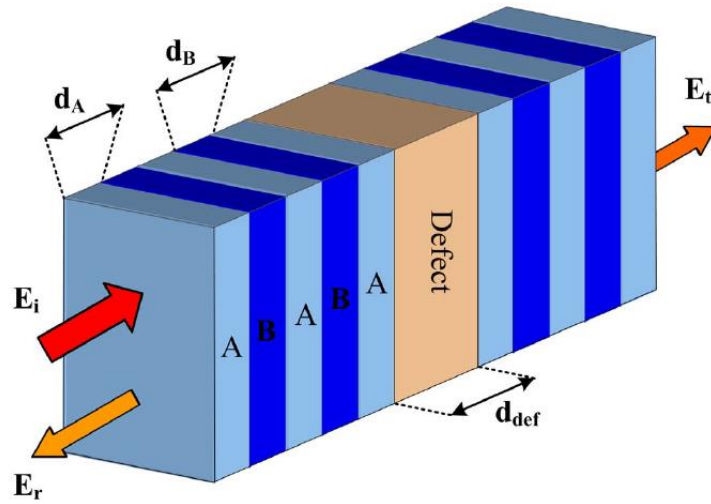


Figure 2.3 A terahertz tag composed of two Bragg mirrors and a central defect.

Source: Bernier, M., Garet, F., Perret, E., Duvillaret, L., & Tedjini, S. (2011). Terahertz encoding approach for secured chipless radio frequency identification. *Applied optics*, 50(23), 4648-4655.

A prototype design containing 2 bits of information was successfully tested for a range of 0.15-0.35 THz, though the authors mention that there are some limitations pertaining to the design of the tag, restricting its applications. These limitations involve the orientation immunity of the tags, as corruptions in the decoding of the defect mode can occur if there is too large a deviation from a straight-on detection of the tag. This is further complicated by the fact that the maximum allowable angle of incidence relative to

the normal to the surface is dependent on the individual tag, and so a standard deviation angle cannot be set. A credit card reader is offered by the author as a possible working application, as the card is locked in place so the orientation can be ensured. The authors also make mention of theoretical improvements to the design to increase storage size using higher-order photonic bandgaps in the Bragg mirrors, as well as recyclable materials that could be used to construct their tag [Bernier et al. 2011].

2.2 Fabrication Methods

A study that has provided guidance in fabrication methods is one by S. F. Busch et al. In this work, the researchers explore the spectral characteristics of many common 3D printable materials in the THz band, as well as a few non-traditional 3D printable materials. Notably, the paper features the refractive indices and absorption coefficients of seven such materials, which are essential in determining which materials are appropriate for the construction of a multi-material tag. The materials tested were Acrylonitrile butadiene styrene (ABS), Polyactic acid (PLA), Nylon, Bendlay, Polystyrene (HIPS), High Density Polyethylene (HDPE) and Polypropylene (PP). The samples were constructed through conventional 3D printing methods, and the properties were tested from 0.2 to 1.5 THz. The relevant results of this study are featured in Table 4.1. [Busch et al. 2014]. As will be discussed in Chapter 4, the material parameters of these materials are used in this thesis to design and fabricate a prototype QR code.

2.3 Deconvolution

In this thesis, deconvolution techniques were applied to accurately determine the location of pulses reflected from the internal geometry of a tag. Some related studies have applied similar THz deconvolution techniques. In a study by Dong et al., THz imaging is utilized in order to complete stratigraphic and subsurface analysis of an art painting. The authors employ a THz frequency-wavelet deconvolution technique to remedy some of the challenges they faced in resolving the features of the chosen painting. One of these issues included not being able to distinguish between separate layers of paint, as they may lack the optical thickness required to register a reflected pulse. The pigments used also can have similar refractive indices, further leading to obfuscations of layer features. A low signal-to-noise ratio was also cited as a potential problem that deconvolution was meant to counteract.

The deconvolution technique first uses frequency-domain filtering and wavelet de-noising methods to improve the signal-to-noise ratio. Their process is shown in Figure 2.4 for filtering done at different cutoff frequencies. The authors were successfully able to reconstruct the stratigraphy of the painting and expressed that this method would likely be effective for other types of stratified systems. X-ray images of the painting were also compared to the THz reconstruction. While similar, the THz imaging was able to pick up many features that X-rays could not. This, in addition to THz radiation being non-ionizing and able to be conducted in reflection, showed the robust potential of THz imaging in the future [Dong et al. 2016].

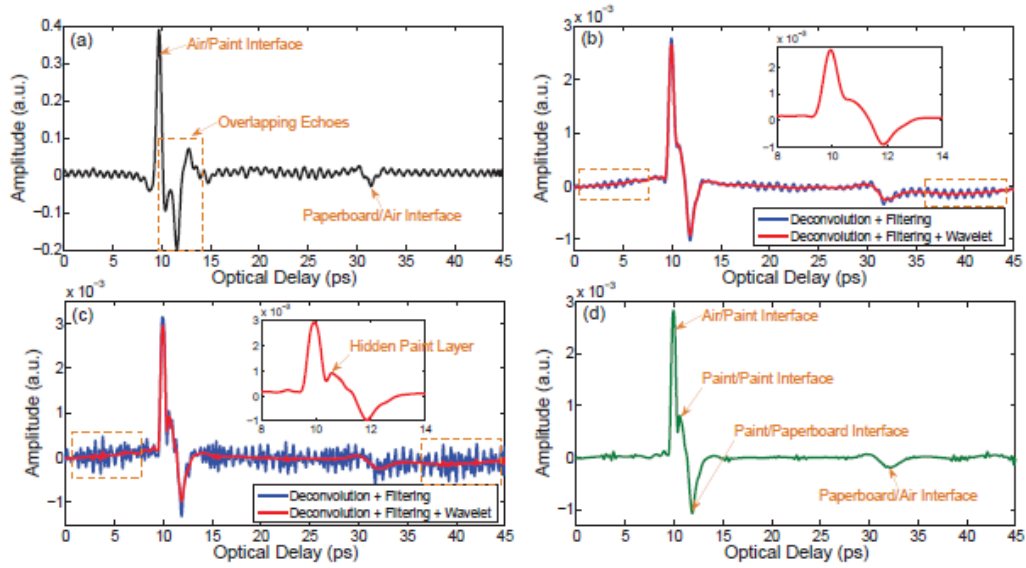


Figure 2.4 THz frequency-wavelet deconvolution result for a typical THz waveform. (a) Original THz reflected waveform from one typical pixel; (b) deconvolution result with frequency cutoff of 2 THz; (c) deconvolution result with frequency cutoff of 3 THz; (d) final deconvolution result to reveal the stratigraphy in this typical pixel.

Source: Dong, J., Jackson J., Melis M., Giovanacci D., Walker G., Locquet A., Bowen J., & Citrin D., (2016) "Terahertz frequency-wavelet domain deconvolution for stratigraphic and subsurface investigation of art painting," *Opt. Express* 24, 26972-26985

CHAPTER 3

RELEVANT TECHNOLOGIES

3.1 Terahertz Time-Domain Spectroscopy

In order to read the 3D QR codes which were produced, time-domain spectroscopy in the Terahertz range was utilized. This method uses pulses of Terahertz radiation that interacts with a sample to produce a waveform representing the internal structure of the sample.

The pulses are generated by a semiconductor with two metal antennas attached to a substrate, which is pictured in Figure 3.1. An ultrafast laser pulse is used to create electron and hole pairs in the semiconductor layer. A voltage bias is applied between the antennas, causing the produced charges to accelerate, and generating Terahertz radiation. The semiconductor has many defects in order to eliminate the photogenerated charges quickly, resulting in a single, sharp pulse of radiation [Mølster 2017].

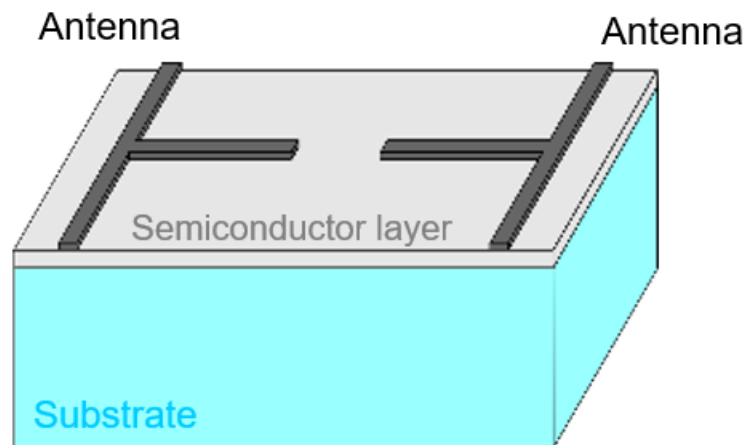


Figure 3.1 The main component of a Terahertz pulse generation device.

Source: TeraMetrix T-Ray 5000 Training Slides (2017)

After a THz pulse interacts with the material under test and propagates to the receiver, the electric field of the pulse provides a bias for the receiver antenna. A receiver optical gating pulse then allows current to flow, which is proportional to the instantaneous THz electric field. This measured current represents the THz instantaneous electric field and is recorded by the Terahertz control unit (TCU). This set-up is depicted in Figure 3.2.

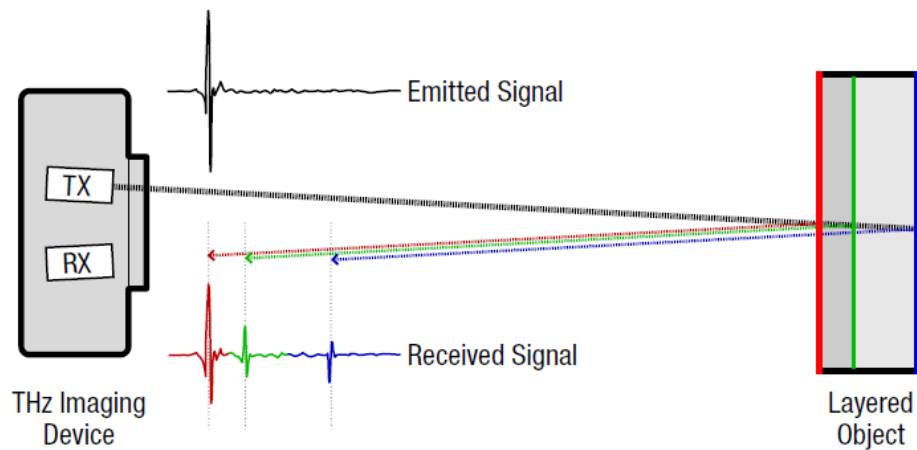


Figure 3.2 A THz imaging device interacting with a sample layered object.

Source: Willis, K. D., & Wilson, A. D. (2013). InfraStructs: fabricating information inside physical objects for imaging in the Terahertz region. *ACM Transactions on Graphics (TOG)*, 32(4), 138.

Measurements of the full THz time-domain waveform are acquired by continuously adjusting the timing delay between the arrival of the THz pulse at the receiver antenna relative to the arrival of the optical gating pulse. An example of a measured waveform is given in Figure 3.3. Measurements can be done using transmission, in which the signal is measured on the opposite side of where the pulse is

produced, or reflection, in which the signal is measured on the same side [Chan et al. 2007].

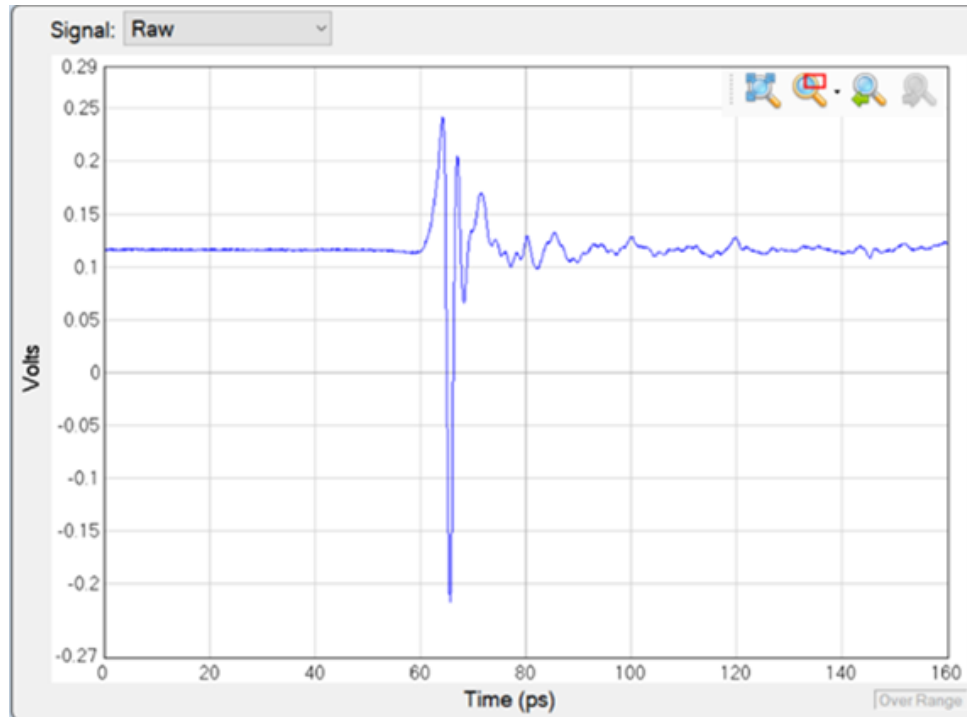


Figure 3.3 An example of a waveform recorded by the Terahertz control unit.

The T-Ray 5000 covers a spectral width of .1-3 THz, which is relatively low energy and non-ionizing. The typical pulse duration is on the order of 3-5 picoseconds. The system operates at 300 GHz [Siegel 2003]. The system uses a pump-probe method of THz imaging, which is the most common technique. This method separates a femtosecond laser pulse into a pump beam and a probe beam. A time delay is created between these beams by adjusting the path lengths of the beam. The pump beam excites the emitter and generates the THz pulse. The pulse travels with the probe beam to the sample to be measured. The amplitude of the pulse is measured based on the time

difference between the pump and probe beams. This process is depicted for different optical lengths in Figure 3.4.

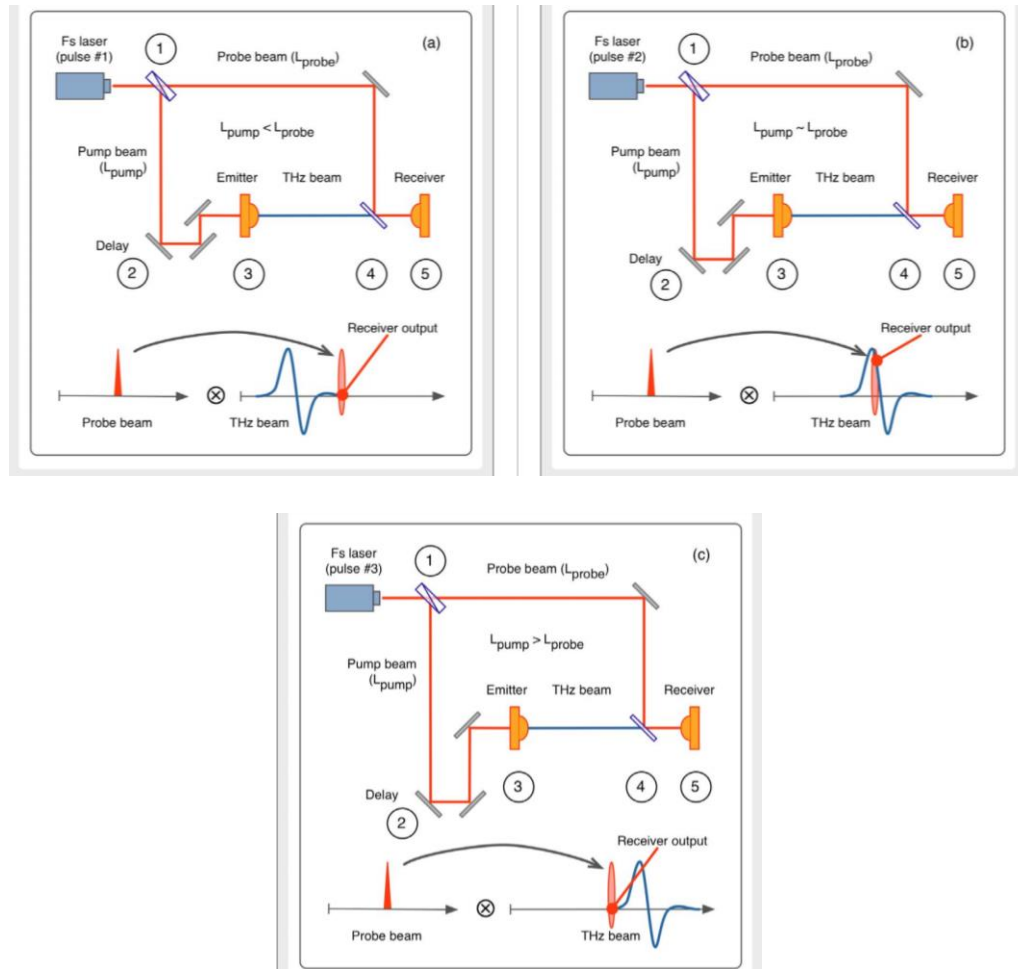


Figure 3.4 Pump-probe layout for when the length of the probe beam is longer than the pump beam (top left), equal to the pump beam (top right), or shorter than the probe beam (bottom).

Source: Redo-Sanchez A. (2012). The Terahertz Wave EBook. Zomega Terahertz Corporation. Apple Books. 6-9.

The Fourier transform of a THz waveform in a logarithmic scale is depicted in Figure 3.5. It is shown that most of the power exists at lower frequencies, with an exponential drop off to the noise dominated section from 1.75 to 3 THz. Other stray pulses can be attributed to atmospheric absorption lines created by water vapor. The drop off that occurs before .1 THz represents the lower frequency detection limit.

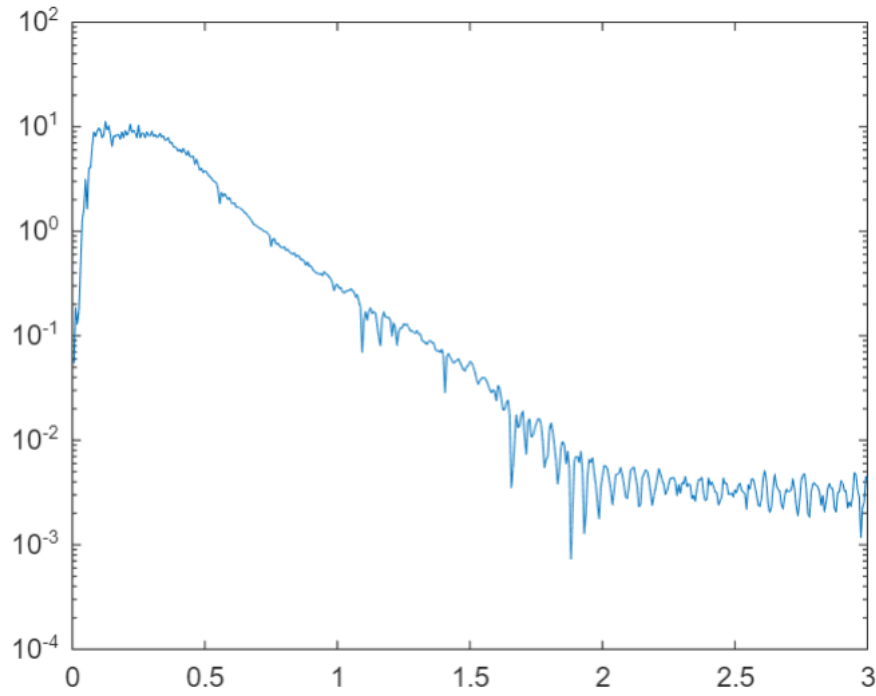


Figure 3.5 Fourier transform of a THz waveform mapped to a logarithmic scale.

For this thesis, a TeraMetrix T-Ray 5000 THz time-domain system was used. The waveform peaks were analyzed to designate which of two materials of different refractive indices lie at different points within the QR Code plastic sample. By analyzing the waveform using deconvolution techniques, and thus identifying the order of the materials, it is possible to output a unique code associated with the sample through a decoding algorithm.

3.2 3D Printing

To construct the 3D QR codes for this study, a 3D Fusion Deposition Modeling (FDM) printer was used. This type of printer works by inputting first a 3D model file created in a

computer-aided design (CAD) program. A reel of plastic filament feeds into an extruder that heats the filament, and the extruder nozzle travels on a movable arm that allows the melted filament to be placed according to the CAD design. The design is printed in individual layers, with each subsequent layer binding and cooling on the layer beneath it (Smyth 2017).

For this thesis, the CAD program utilized was Autodesk Fusion 360. The 3D printer used was the Ultimaker 3, which has two separate extruders. This allows two different plastics to be printed as part of a single object, allowing more diversity in the type of designs that can be constructed.

3.3 Deconvolution Processing

Deconvolution in the THz time-domain is the process of detangling the components of the reflected electric field. The convolution of the signal is given by the following equation:

$$r(t) = i(t) \otimes h(t). \quad (3.1)$$

Here, $r(t)$ is the reflected electric field, $i(t)$ is the incident THz pulse, and $h(t)$ is the impulse response function (Dong et al. 2016). In deconvolution, the objective is to isolate the impulse response function, as it contains the desired information about the features of the object being studied. This can be done by using an inverse Fourier transform as follows:

$$h(t) = FFT^{-1} \left[\frac{FFT(r(t))}{FFT(i(t))} \right] . \quad (3.2)$$

In this equation, FFT and FFT^{-1} represent the Fourier transform and inverse Fourier transform respectively. In effect, this function should result in refined impulses representing the reflections from the internal structure of a sample (Dong et al. 2016).

For this study, deconvolution is used to accurately measure where the material interfaces lie within a sample. The TeraMetrix T-Ray 5000 uses a noise and metal reference measurement to aid in its deconvolution analysis. A comparison of the raw and deconvolved waveforms is shown in Figure 3.4. By utilizing deconvolution, the timing between pulses can be ascertained, indicating where material transitions did and did not occur. Thus, the deconvolved waveform is congruent with the material layering of the sample structure. Deconvolution mitigates ‘pseudo-pulses’ generated from noise, making the waveform data more reliable. This is especially relevant when applying the decoding algorithm for this study to the waveforms, as minor voltage fluctuations misidentified as pulses will lead to an incorrect output of the intended binary code. The way in which the deconvolved waveforms are employed is discussed in more detail in Sections 5.3 and 5.4, with the decoding process being explored in Section 6.1.

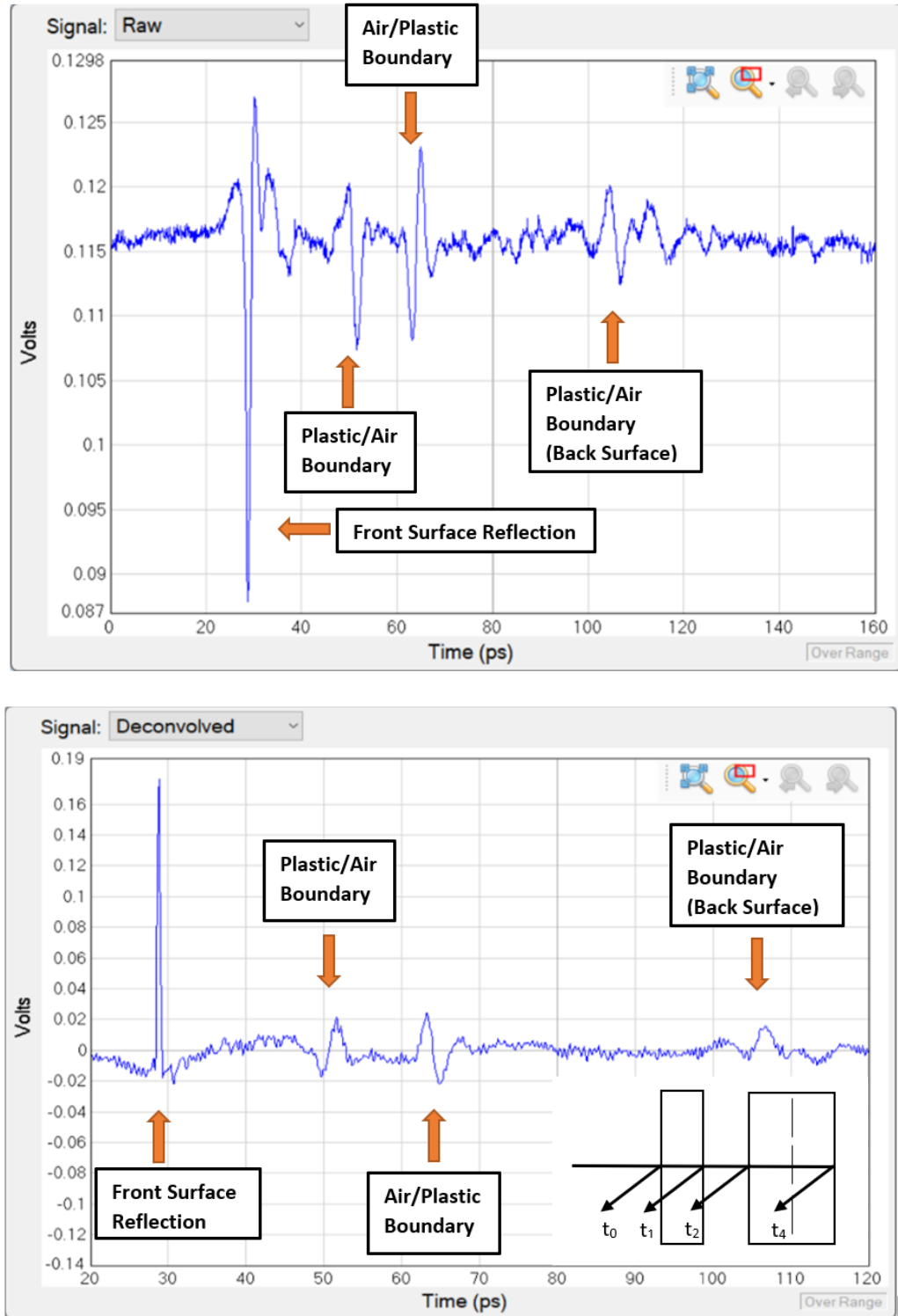


Figure 3.6 An example of a raw waveform from a 3D QR code pixel (top) and its deconvolved counterpart (bottom). An illustration depicting the pixel and its reflection locations is also depicted (bottom right).

CHAPTER 4

OPTICAL THEORY

4.1 Refractive Indices

The materials chosen to create a tag are one of the greatest factors in producing a consistent output code. Every material has an associated real index of refraction that represents a ratio of the speed of electromagnetic radiation in vacuum to the speed of electromagnetic radiation in the chosen material.

All materials also have an associated absorption coefficient, which governs how efficiently a particular wavelength can propagate through a material before being absorbed. This can be calculated with the following equation:

$$\alpha = \frac{4\pi k}{\lambda}. \quad (4.1)$$

Here, α is the absorption coefficient, k is the absorption index (or the imaginary component of the index of refraction), and λ is the wavelength [Brillouin 1953]. Since this study is limited to wavelengths in the THz region, the absorption coefficient must be considered solely based on the material.

The results related to the study discussed in Section 2.2 are given in Table 4.1. This table provides the refractive indices and absorption coefficients of some common materials used in additive manufacturing.

Table 4.1 Printing and Material Parameters of Common 3D Printed Materials at 500GHz

Material	Printing Temperature [°C]	Sample Thickness [mm]	Refractive Index n @500 GHz	Absorption Coefficient [cm⁻¹] @500 GHz
ABS	250	1	1.57	5
PLA	220	1	1.89	11
Nylon	255	1	1.72	9
Bendlay	250	5	1.532	1.8
Polystyrene	240	5	1.561	0.5
HDPE	230	5	1.532	0
PP	230	5	1.495	0

Source: Busch, S. F., Weidenbach, M., Fey, M., Schäfer, F., Probst, T., & Koch, M. (2014). Optical properties of 3D printable plastics in the THz regime and their application for 3D printed THz optics. Journal of infrared, millimeter, and Terahertz waves, 35(12), 993-997.

The Fresnel equation for calculating how much radiation power is reflected when passing from one medium to the other is given as:

$$R = \left(\frac{n_1 - n_2}{n_1 + n_2} \right)^2. \quad (4.2)$$

In the above equation, R represents the reflected power from radiation incident from material 1 to material 2. The n_1 and n_2 represent the indices of refraction for the incident and refracted mediums respectively. After radiation crosses the boundary into material 2, the amount of transmitted electromagnetic radiation which propagates through a distance in material 2 is given by:

$$T = se^{-ab}. \quad (4.3)$$

For this equation, $s = 1 - R$ represents the initial amount of radiation in material 2, a is the absorption coefficient (in terms of power) of the material, b is the thickness of material 2, and e is Euler's number [Willis & Wilson 2013].

In constructing 3D QR codes for this study in which relatively small thicknesses are used, the difference in refractive indices was maximized in order to produce the strongest signal possible. If more layers were added to make a more robust code, reducing the difference in refractive indices may be necessary for the signal to propagate to the final layer.

Another factor that must be considered in regard to thickness is the absorption coefficient of each material, as it sets the theoretical limit for the maximum depth of a tag. A higher absorption coefficient necessitates that the THz wave attenuates more quickly and thus the measured signal is weaker. A tag that is too deep will not be read correctly, as the THz radiation will degrade too quickly to reach the farthest layers of the tag.

Beyond the theoretical, the depth of the tag in experimentation will most certainly need to be reduced further, as the signal-to-noise ratio of the pulses may make it difficult to discern where pixels are actually located, as they will blend with the noise. While in principle a tag can be made from any 3D printable material, the depth must be chosen to be safely below this theoretical limit.

One final aspect of the QR code to assess is the lateral pixel size. Since a THz wave has an associated beam diameter, there exists a theoretical minimum pixel size. If the beam diameter surpasses the pixel size, unwanted reflections or scattering of THz radiation from the lateral boundaries of the pixel may occur which would disrupt the data collection and decoding processes.

The THz waves used in this study can be approximated as a Gaussian beam, where the amplitude and irradiance profile in the transverse plane follows a Gaussian distribution. This means the intensity of the beam is mainly focused around the beam axis, and can be concentrated to one spot (namely, a pixel). When a Gaussian beam interacts with a circularly symmetric lens centered along the beam axis, a new Gaussian beam is formed [Saleh & Teich 1991].

The waist radius of a Gaussian beam is the minimum radius of the beam before diverging due to diffraction. When a lens is placed at the waist radius of an incident beam, the waist radius of the transmitted wave is given by:

$$W'_0 = \frac{W_0}{\sqrt{1 + \left(\frac{z_0}{f}\right)^2}} \quad (4.4)$$

In this equation, W'_0 and W_0 are the waist radius of the transmitted and incident beam respectively, z_0 is the depth of focus for the incident beam, and f is the focal length of the lens. For instances where the depth of focus is much larger than the focal length of the lens, this can be approximated using the following:

$$W'_0 = \frac{\lambda}{\pi W_0} f. \quad (4.5)$$

Here, λ signifies the wavelength of the Gaussian beam. This equation illustrates that the beam diameter can be minimized by decreasing the wavelength and focal length of the lens, while increasing the initial beam diameter before it is focused by the lens [Saleh & Teich 1991].

For this study, the wavelength was restricted to the THz domain, and there was limited control over the incident beam from the apparatus utilized. Thus, the main control over beam diameter was found in manipulating the focal length of the lens used. In experimentation, it can be expected that the pixel size must be securely larger than the minimum beam diameter, as diffraction of the beam will lead to diameter growth as it propagates. This can be observed in the difficulties mentioned in Section 5.2.

The Rayleigh range, z_R , is defined as the distance from the beam waist to the point where the cross-sectional area of the beam doubles. Effectively, it is half the range for which the beam maintains its pixel size before diffracting significantly. It can be found using the following equation (with variables defined earlier):

$$z_R = \frac{\pi W_0^2}{\lambda}. \quad (4.6)$$

4.2 Waveform Analysis

The signals acquired through time-domain spectroscopy represent a volumetric representation of the object being measured. The peaks of each waveform show the amplitude of reflected radiation against the time-of-flight (TOF) for the pulses. In a

structure containing two materials, it is expected that a peak of high amplitude would be reflected from the boundary when the refractive indices of the two materials are significantly different. When the two refractive indices are equal, no reflected pulse is generated at the boundary. The algebraic sign of the amplitude depends of whether the light is propagating from a lower to higher refractive index material or from a higher to lower refractive index material. When a pulse is reflected from a higher refractive index material, the amplitude of the pulse is inverted, while a reflection from a lower refractive index material leaves the reflected pulse noninverted.

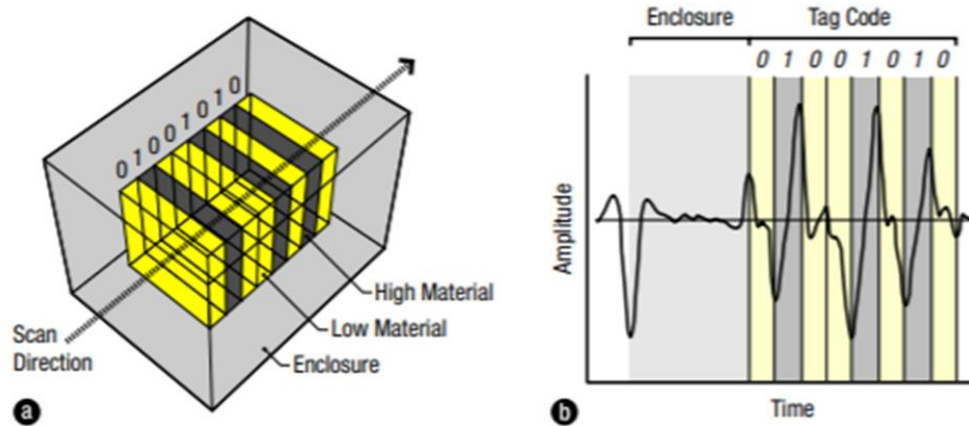


Figure 4.1 An example of a THz pulse interacting with a sample tag. The left side depicts the scan direction and configuration of two materials. The right side (the incoming pulse has a positive amplitude) shows the reflected waveform produced by the pulse interacting with the material layers. Note that when the pulse interacts with a boundary between a 0 and 1 (low to high refractive index), the amplitude of the pulse is inverted.

Source: Willis, K. D., & Wilson, A. D. (2013). InfraStructs: fabricating information inside physical objects for imaging in the Terahertz region. *ACM Transactions on Graphics (TOG)*, 32(4), 138.

In creating a 3D QR tag, the amplitudes of the peaks as well as their positions in time can be used to extract the intended code from the internal geometry of the structure.

The high positive or negative amplitude peak represent a transition between a binary '1' to '0' or a binary '0' to '1'. A missing or low amplitude peaks represents a binary '0'-'0' or '1'-'1' boundary. The initial amplitude (i.e. positive or negative) of the incoming THz pulse can be determined by the positive or negative amplitude of the first reflected pulse from the tag. As long as the nominal thickness and refractive indices of the QR code materials are known, it is possible to utilize the waveform dataset to output the code embedded in the material layering.

CHAPTER 5

3D TERAHERTZ QR CODE

5.1 Design

The 3D THz QR codes produced for this study were designed in the CAD software Autodesk Fusion 360. The 3D printing program Ultimaker Cura was used to slice the designs in preparation for printing. The Ultimaker 3 was the 3D printer used to manufacture the designs.

Polylactic acid (PLA) was chosen as the material used to create the tags. In Table 4.1 it was shown that PLA has a relatively high refractive index that contrasts greatly from that of air, meaning the waveforms peaks produced at their boundaries are strong enough to be clearly determined. PLA is also one of the most commonly used 3D printing materials, as it is widely available, cheap, and has reliable dimensional accuracy (Smyth 2017). While PLA is listed as having the highest absorption coefficient out of the given materials, this is taken into account as the depth of the tags produced are less than half the size where the attenuation of the electric field would become a significant problem, as calculated using the equations in Section 4.1. Also, a functional PLA THz tag represents a boundary for which materials with lower absorption coefficients and similar refractive indices would almost certainly be functional as well. If a tag with significantly more depth were to be constructed, a material with a lower absorption coefficient and refractive index would most likely want to be chosen.

Polypropylene (PP) was considered as an alternative material for this study, as it effectively has a negligible absorption coefficient, but it is also known to be a

substandard 3D printing material. PP is an extremely soft plastic with no clearly defined melting point and an unusually high temperature expansion coefficient [Busch et al. 2014]. For these reasons, PP was not an ideal candidate for the designs needed in this study.

Many different types of designs were prototyped during the course of this study, but only two will be discussed in detail here, with one being the precursor to the other. The first is known as the ‘uncovered’ design, and the second is the ‘clandestine’ design, which can be seen in Figures 5.1 and 5.2 respectively. Each will be discussed in their relevant sections (Sections 5.3 and 5.4), but the essentials of each are the same.

The 3D QR codes feature a stratified design, with each layer being 4 cm in length and width. Some of these layers were solid PLA, while others contained 1 cm by 1 cm pixels arranged in a 3 by 3 array. These pixels were either ‘filled-in’ with PLA, or instead an air gap within the structure. A PLA pixel represents a binary ‘1’, while an air gap represents a binary ‘0’. Each tag featured two encoded layers, meaning that the final output represents an 18-digit binary code, though this can be extended by adding more layers. While the selected dimensions are somewhat arbitrary, prototyping revealed this to be a good balance between being so large that it is cumbersome, and too small to precisely identify pixels.

A depth of either 2.5 mm or 2 mm was used for each layer of the tag (depending on the version), which was chosen for a few reasons. As mentioned earlier, this guaranteed that attenuation would not be a notable issue for the largest tag produced, which was four layers and 8 mm deep. A more prominent reason came in the form of how the TeraMetrix T-Ray 5000 Terahertz time-domain system used in this study

collects data. The time window for the T-Ray 5000 system is 160 picoseconds, meaning that all the pulses collected from a given tag must fit within that time constraint. While the start of this window may be adjusted, tags with too large of a depth may lose significant pulse features if they extend beyond the 160 ps recorded time range. In practice, pulses outside the time window would also sometimes ‘wrap around’ to the front of the time window during the deconvolution calculation, putting later pulses before earlier ones and disordering the data set. While it could be possible to reorder the data set, it added an unnecessary complication to the decoding process that could simply be solved in the design of the tag.

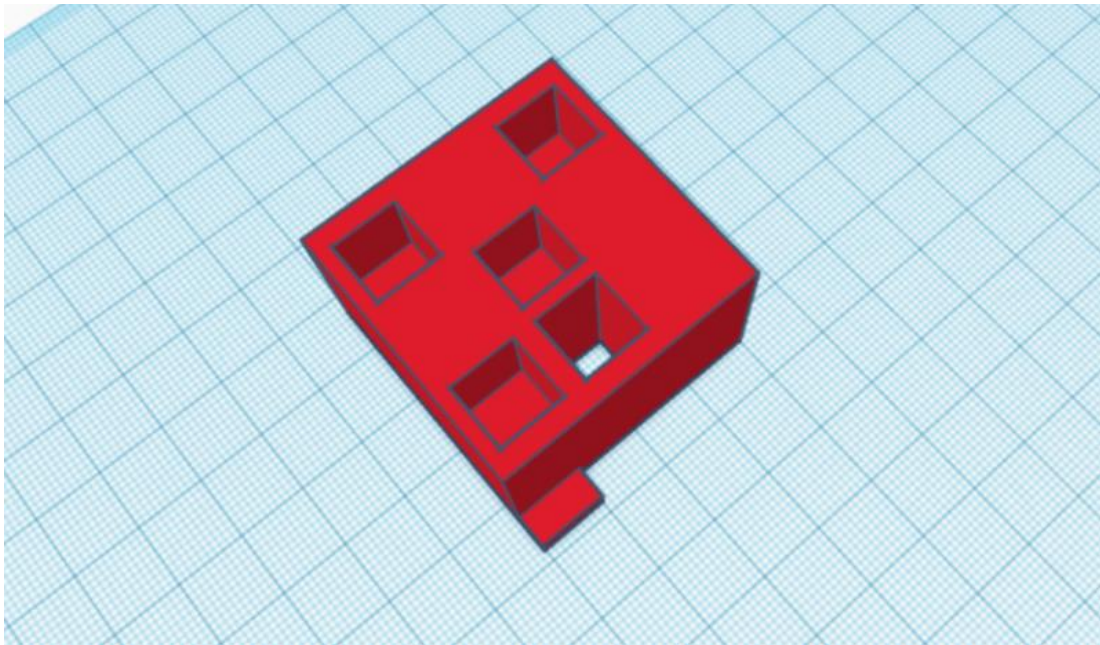


Figure 5.1 Uncovered 3D QR Code as seen in CAD software.

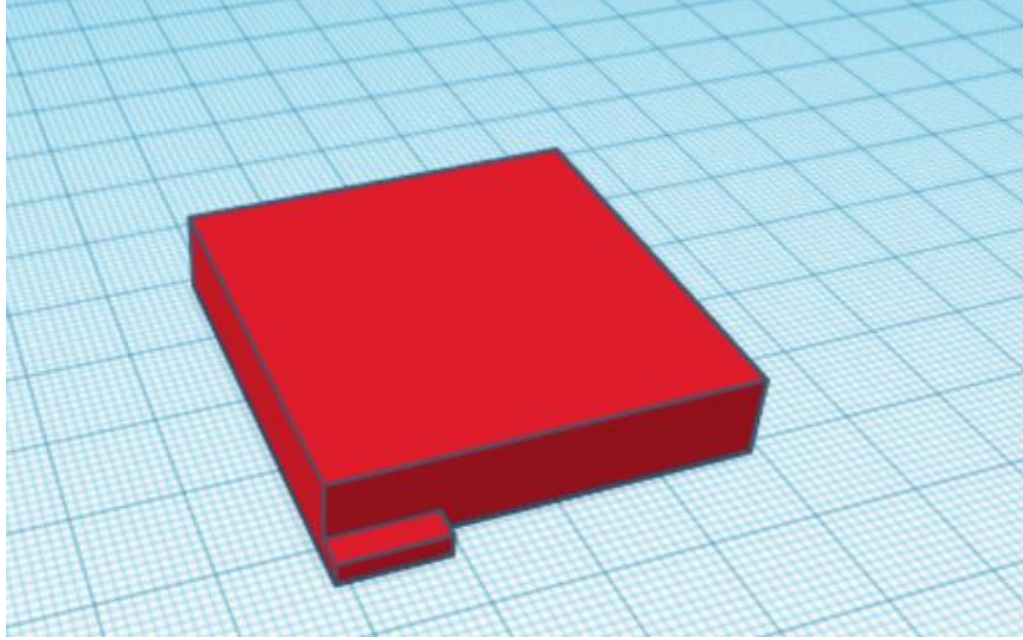


Figure 5.2 Clandestine 3D QR code as seen in CAD software.

For the tag designs featured in this study, each layer was printed together as one fully adjoined 3D print. In prototyping, it was determined that combining layers with adhesives and/or refractive index matching materials would often lead to unwanted reflection features which may be incorrectly identified as pulses. Thus, it was seemingly necessary to print the layers together to avoid unwanted reflections. Luckily, due to the relatively small size of each pixel, bridges could be printed over air gaps within the structure without damaging the overall structural integrity.

Designs were also prototyped that featured two 3D printed plastics as opposed to an air gap, which were printed together using the dual extruders of the Ultimaker 3. Unfortunately, through preliminary experimentation, it appeared as though there are no two commonly used 3D printable materials with distinctive enough refractive indices to give reliable pulses between interfaces.

Finally, each tag features a small protrusion on one side of its bottom layer. This is done so that the orientation of the tag can be easily identified as to not confuse pixel locations, because the tag is symmetrical otherwise.

5.2 Data Collection

All tags created in this study were measured using the same general procedure. A TeraMetrix T-Ray 5000 Terahertz time-domain system was used to generate and measure THz waveforms in reflection mode.

While THz imaging can be done in transmission, for the application explored in this study, this mode would be impractical. Resolving a wave that has passed through a sample rather than just its reflections makes it much more difficult to determine the exact location of surface boundaries, as the recorded wave will have passed through the entire sample resulting in a potentially large attenuation of the beam compared to a reflection geometry. Moreover, a transmission geometry requires two internal reflections for the presence of each interface to be manifested in the transmitted waveform while a reflection geometry only requires one internal reflection. Also, having a receiver on the opposite side of the tag may be impossible in practical applications, as it may be part of an object that is too thick to avoid full attenuation.

Before collecting data, the system requires a reference and background/noise sample be collected first in order to refine the data recorded through experimentation. For a reference waveform, a mirror was used to simulate an ideal reflection, while simply covering the THz imaging device was sufficient for noise and background waveforms.

The tag was then secured in front of the THz imaging device using a standard optomechanical post assembly and mount. This configuration can be seen in Figure 5.3.

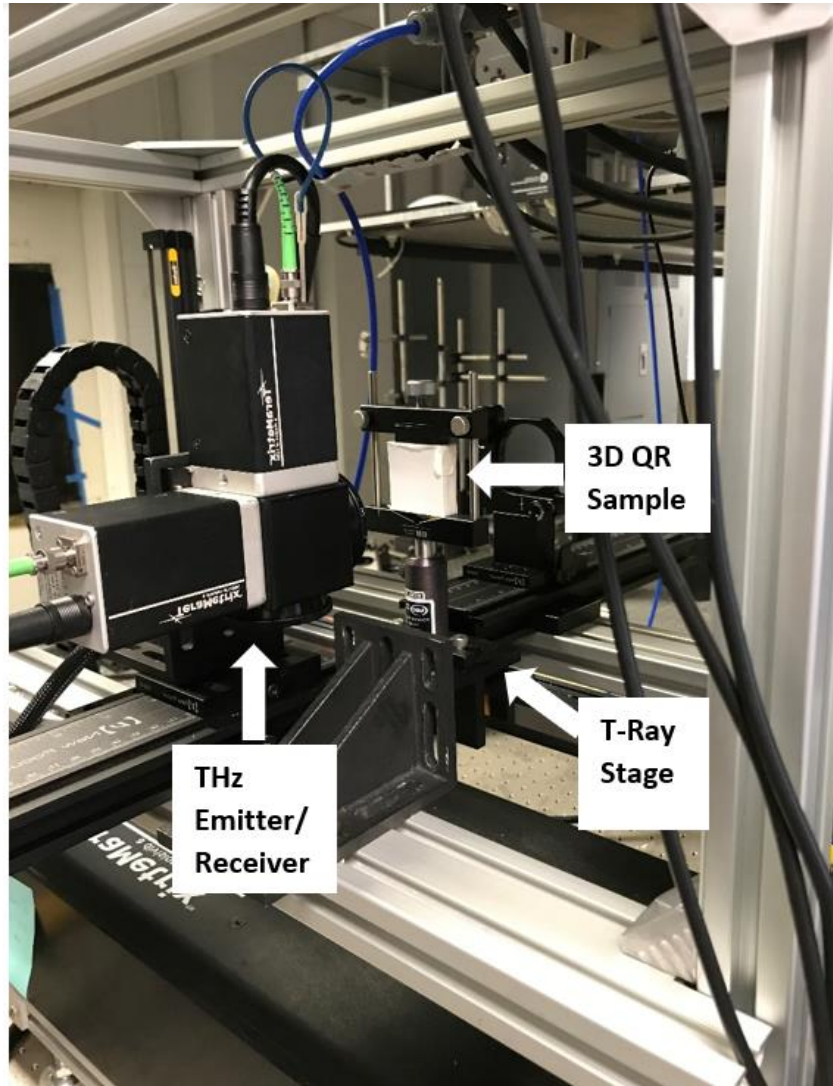


Figure 5.3 A sample 3D QR tag mounted in front of THz imaging device.

At first a 6-inch lens was used in the THz imaging system to collect data, but this seemed to introduce extra reflection features that could be interpreted incorrectly as pulses within the tag's structure. This was most likely due to a large beam diameter of the

Gaussian beam, as discussed in Section 4.1. While a 6-inch lens may work fine for a tag with larger pixels, the tag then becomes less clandestine, which is part of the purpose of this study. Thus, a 3-inch lens was utilized, as it provided an experimental beam diameter and resolution appropriate for the tags in question. Using Equation 4.5, the spot size of the focused THz radiation was found to be approximately 4.8 mm for a 3-inch lens. This is assuming a wavelength of 3 mm and an incident beam diameter of 8 mm.

In calculating the Rayleigh range for the T-Ray 5000, we get a distance of 70 mm. This used the same assumptions as the previous calculation. Doubling this, we get a total viable range of 140 mm for which the code can exist in before diffraction becomes a major consideration.

In using the T-Ray 5000, a ‘recipe’ must also be established in order to perform THz imaging. For this study, the frequency power integration of the sample was chosen as the imaging parameter, and was done in the .1-2 THz, .5-2 THz, 1-2 THz, and 1.5-2 THz ranges. The clearest image of pixel locations was used to determine waveform measurement locations. An example of defining a recipe can be observed in Figure 5.4. The recipe may also be used to aid the system in identifying relevant pulses for the deconvolution calculation that the system performs. Setting a recipe entails defining the approximate time windows (shown as the #1 and #2 boxes in the top of Figure 5.4) and amplitudes one may expect to find a pulse given the internal geometry of the measured structure. For the purposes of this thesis, the recipe was used to generate a 2D imaging in the 1.5-2 THz spectral range to locate the center positions of each pixel. After moving to the center positions of the pixel, a deconvolved waveform was saved for each pixel location. The extraction of the QR code from the deconvolved waveform for each pixel

location was accomplished using a custom MATLAB code described in Section 6.1 of this thesis.

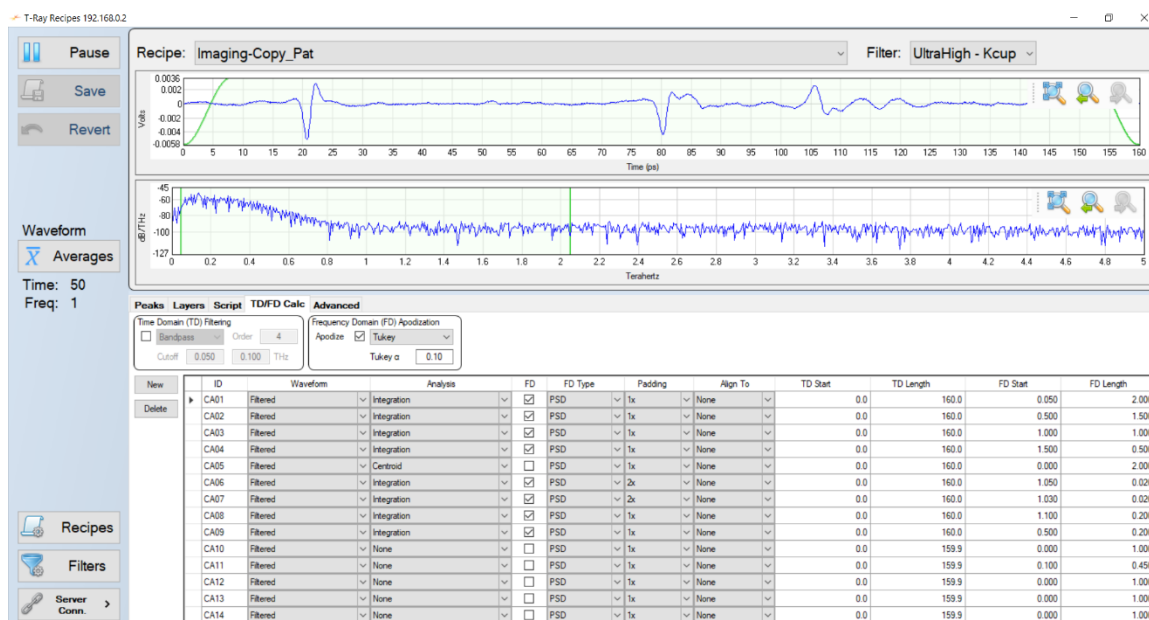
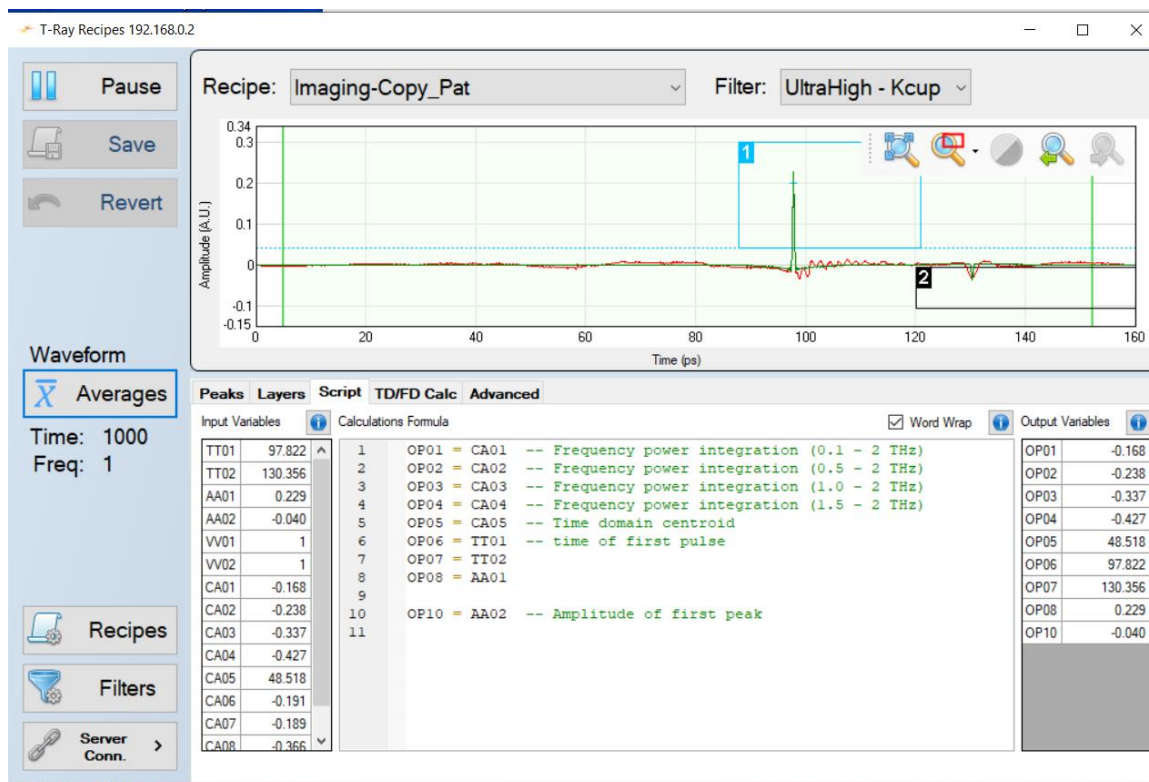


Figure 5.4 An example of the script for a recipe on the T-Ray 5000 (top) and the time-domain and frequency-domain filtering applied (bottom).

In order to identify the pixel locations, a low-resolution image scan of the tag was acquired in the 1.5-2 THz spectral range. This was done by manually adjusting the stage

of the T-Ray 5000 system independently on the x- and y-axis, looking at the waveform display to find the approximate locations where the THz imaging device firstly and lastly interacts with the tag, then setting these as the scanning bounds. Once the bounds were set, the system would automatically perform the scan pixel by pixel, row by row. A high scan rate/low-resolution could be used, as the purpose of this is to simply identify where the embedded pixels are located within the structure perpendicularly to the scan axis. One such scan can be seen in Figure 5.5. Since the 2D image clearly defines the lateral spatial location of the pixels, it was then possible to manually select the stage position so that it lined up with the individual pixel to be measured.

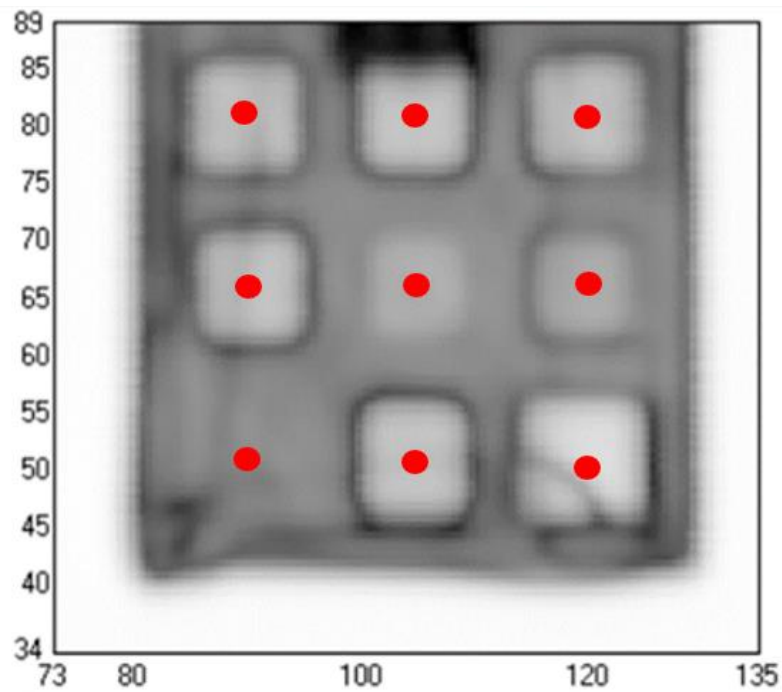


Figure 5.5 An example of an image taken of a 3D QR code tag in the 1.5-2 THz range. Red dots signify approximate positions where pixel waveform data was taken.

Each pixel's raw waveform was measured and recorded. A feature of the T-Ray 5000 allowed multiple waveforms to be averaged in one location, giving a resultant

waveform that minimized random errors. The system was also able to automatically apply a deconvolution to each waveform, generating an output with relatively crisp pulses. Once every pixel was accounted for, the data collection process was terminated.

5.3 Uncovered QR Code

The first 3D QR code to be discussed is the ‘uncovered’ variety. This tag has only two layers, both of which are encoded with pixels. This means that the code is visible to an outside observer, and acts as a preliminary iteration to the fully clandestine tag to be discussed in the following section. Another clear disadvantage of this tag is there is no front surface to use as reference, which was taken into account and improved upon in the succeeding tag version. The reason this tag was tested first was to be sure that such a code could be visually decoded from its waveforms without the complications of a front and back surface. The tag was designed to feature each type of pixel permutation to demonstrate how each would appear as a waveform.

This tag was constructed with 2.5 mm layers for a total depth of 5 mm. Using the basic index of refraction and velocity equations, the approximate time it takes THz radiation to travel through a single layer can be determined. Using an index of refraction for PLA of 1.89 through a 2.5 mm layer, it can be calculated that it will take roughly 16 picoseconds for the wave to propagate through. Since measurements are taken in reflection, this would represent about a 32-picosecond delay between pulses, as it must pass through the layer twice. Similarly, for an air layer we can determine the delay between pulses to be approximately 17 picoseconds.

For a pixel where the first layer is air and the second layer is plastic (or a ‘01’ pixel), it is expected that there is a large front reflection pulse, and a second smaller inverted pulse approximately 32 picoseconds later, as the wave will attenuate through the PLA. This can be seen in the deconvolved waveform in Figure 5.6.

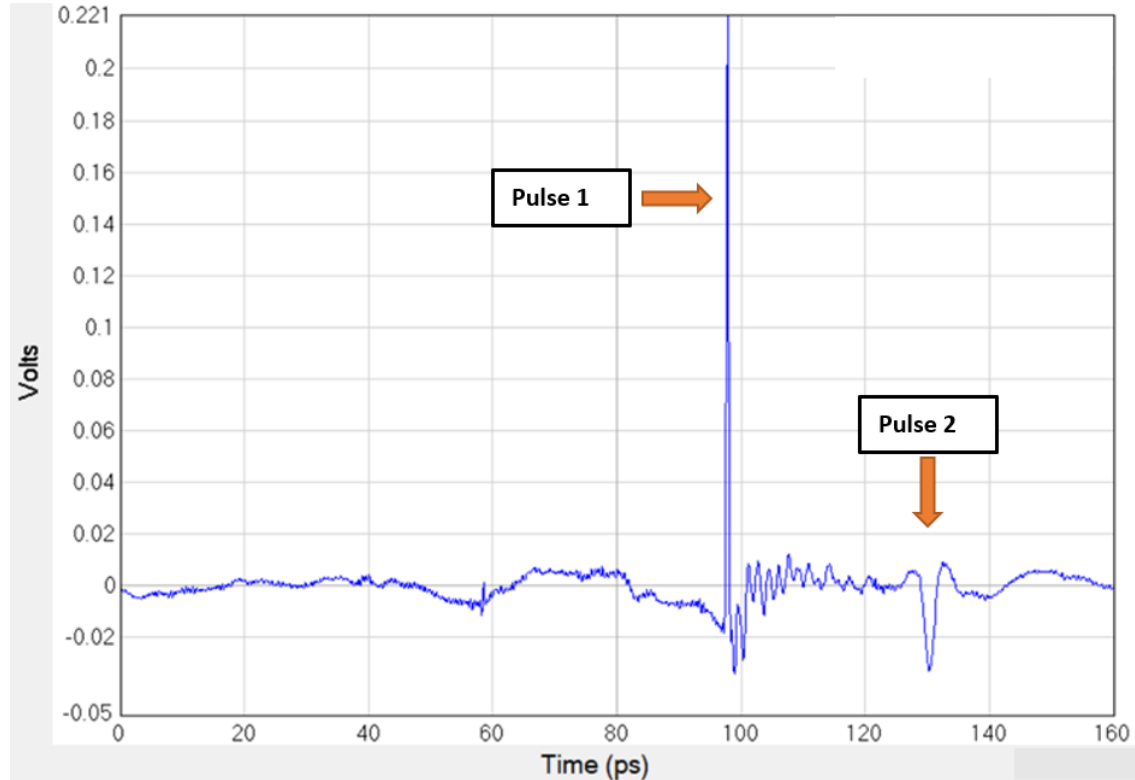


Figure 5.6 An example of a ‘01’ pixel for the uncovered tag as a deconvolved waveform.

For a pixel where the first layer is plastic and the second layer is air (or a ‘10’ pixel), it is expected that the interval between the two pulses is identical to the ‘01’ pixel, but each pixel should be shifted approximately 17 picoseconds earlier, as it hits the front surface a layer sooner. This highlights a major flaw in not having a front surface, as the time window can be adjusted, so it must be confirmed that every pixel is measured within

the same exact conditions. An example of this type of pixel as a deconvolved wave can be seen in Figure 5.7.

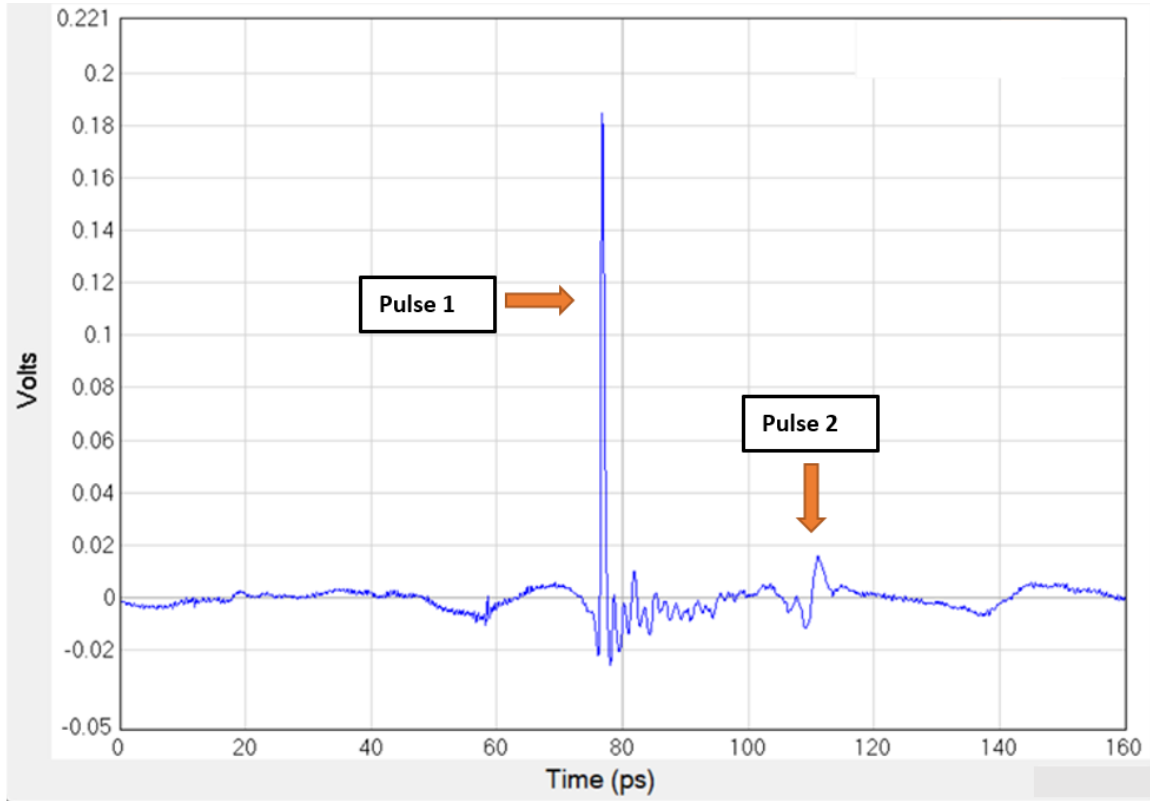


Figure 5.7 An example of a ‘10’ pixel for the uncovered tag as a deconvolved waveform.

For a pixel that has both layers filled with plastic (or a ‘11’ pixel), a time delay of approximately 64 picoseconds between the two pulses is expected, as the wave must now travel through two plastic layers. This can be seen as a deconvolved waveform in Figure 5.8.

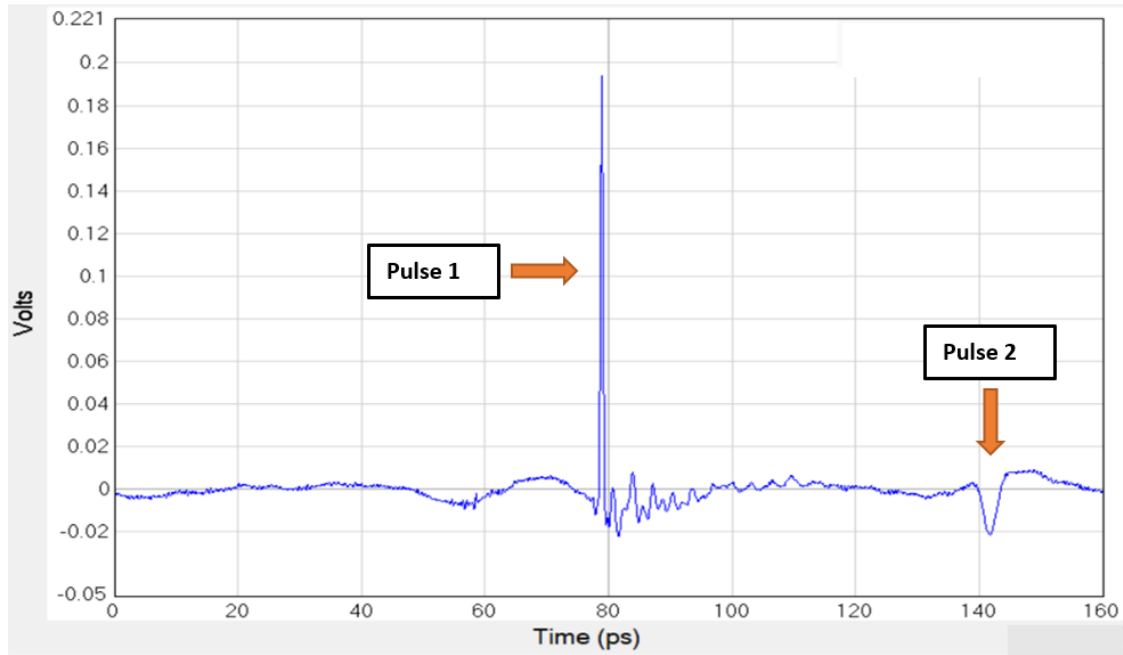


Figure 5.8 An example of a ‘11’ pixel for the uncovered tag as a deconvolved waveform.

Finally, for a pixel that has two air gaps, it is clearly expected that there will be no pulses, and so only noise is expected in the waveform. This can be observed as a deconvolved wave in Figure 5.9.

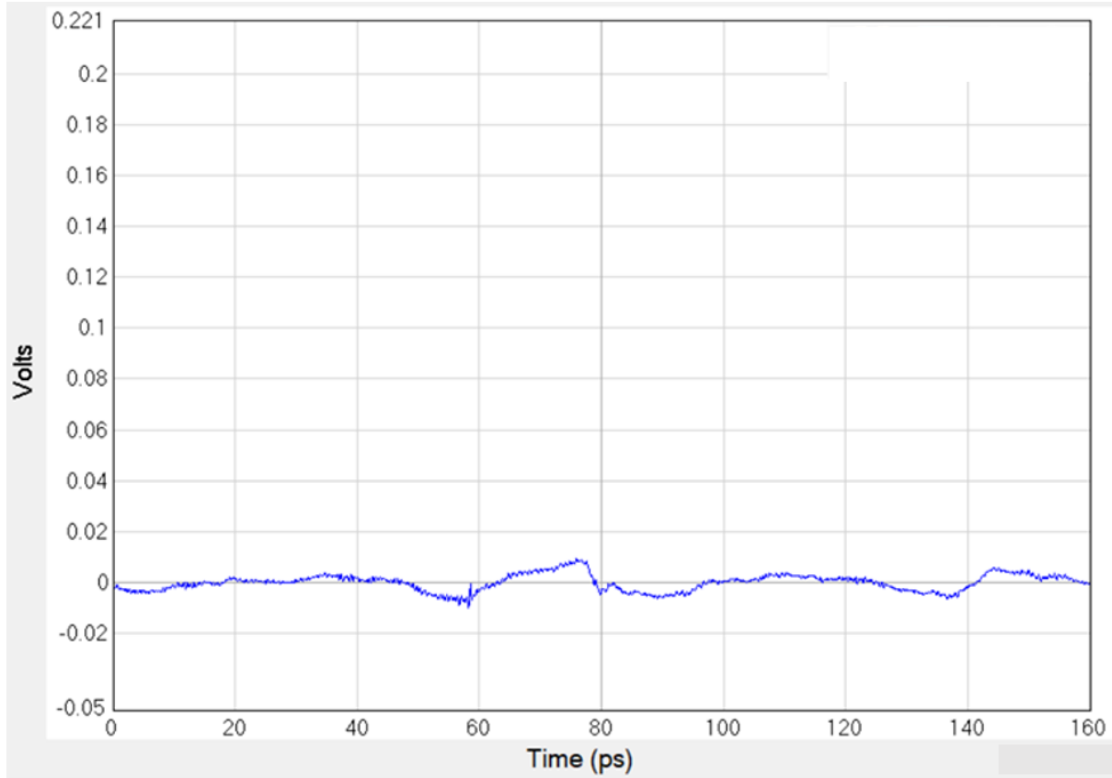


Figure 5.9 An example of a ‘00’ pixel in the uncovered tag as a deconvolved waveform.

5.4 Clandestine QR Code

Improving on the initial design, a fully clandestine QR code was constructed. In addition to the two encoded layers from the previous design, an additional fully plastic layer was adjoined to the top and bottom of the tag during the 3D printing process. This was to hide the internal structure of the tag and consequently the code it represented, as well as to provide a consistent front surface that can be used as reference in decoding pixels.

For this tag, the depth of each layer was reduced to 2 mm to ensure that all pulses would fit within the T-Ray 5000’s time window. Once again, using the basic refractive index and velocity equations, the time to pass through a single layer can be found. For a 2mm PLA layer, it takes approximately 11 picoseconds for a THz wave to pass through

one-way, or 22 picoseconds after being reflected. For an air layer, it would take approximately 6.67 picoseconds to pass through one-way, or 13.34 picoseconds reflected.

It is important to emphasize that the time duration of a ‘bit’ in the QR code structure is not fixed but instead depends upon the speed of light in the medium. This is in contrast to standard digital fiber-optical communication systems in which the time duration of one bit of information is fixed regardless of whether the bit is a ‘0’ or a ‘1’.

In the subsequent chapter, the conception and application of a decoding algorithm to output a binary code from this tag will be explored. For the remainder of this section, a visual decoding will be done similar to the previous section.

For a pixel with an encoded air layer followed by a plastic layer (or a ‘01’ pixel), a large pulse from the front surface would be expected, then a 22-picosecond gap to the next pulse as it transitions from plastic to air. Next would be a 13.34-picosecond gap to when it transitions back to plastic, and finally a 44-picosecond gap after traveling through two plastic layers to the back surface. This can be seen as a deconvolved waveform in Figure 5.10.

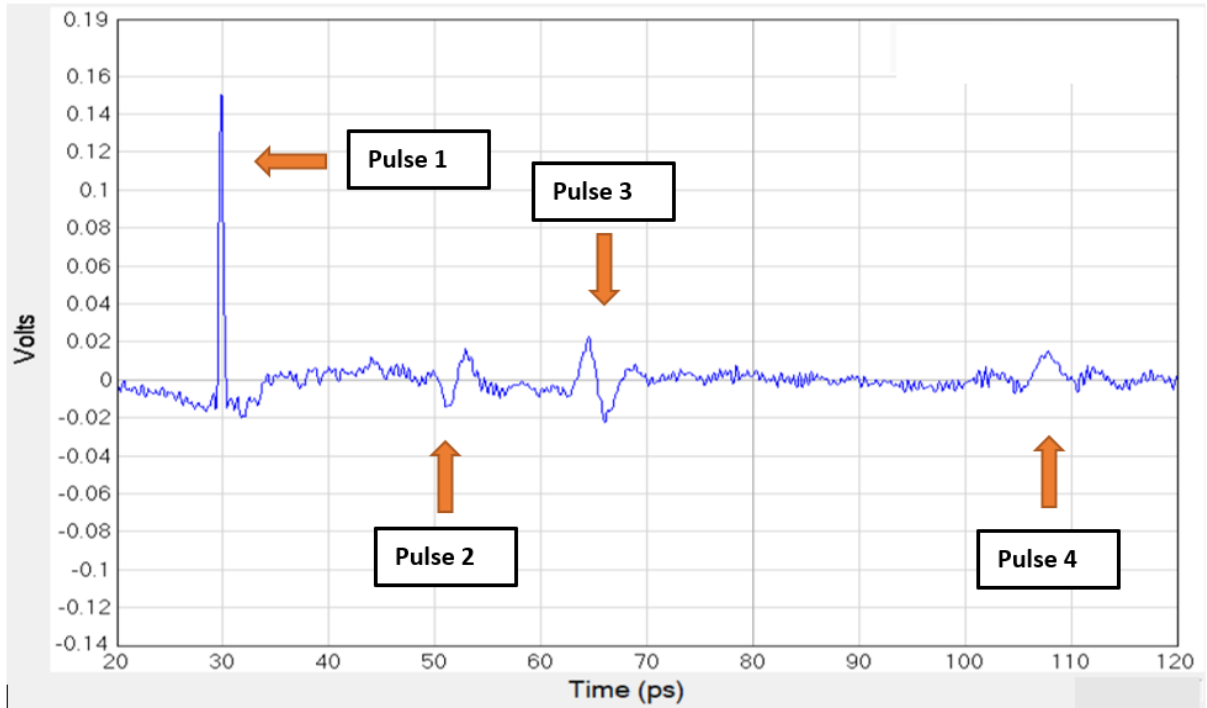


Figure 5.10 An example of a ‘01’ pixel in the clandestine tag as a deconvolved waveform.

For a pixel with an encoded plastic layer followed by another plastic layer (or a ‘11’ pixel) , a pulse is expected off the front surface, followed by a 88-picosecond gap as it travels through 4 plastic layers before reaching the back surface. This can be seen as a deconvolved wave in Figure 5.11.

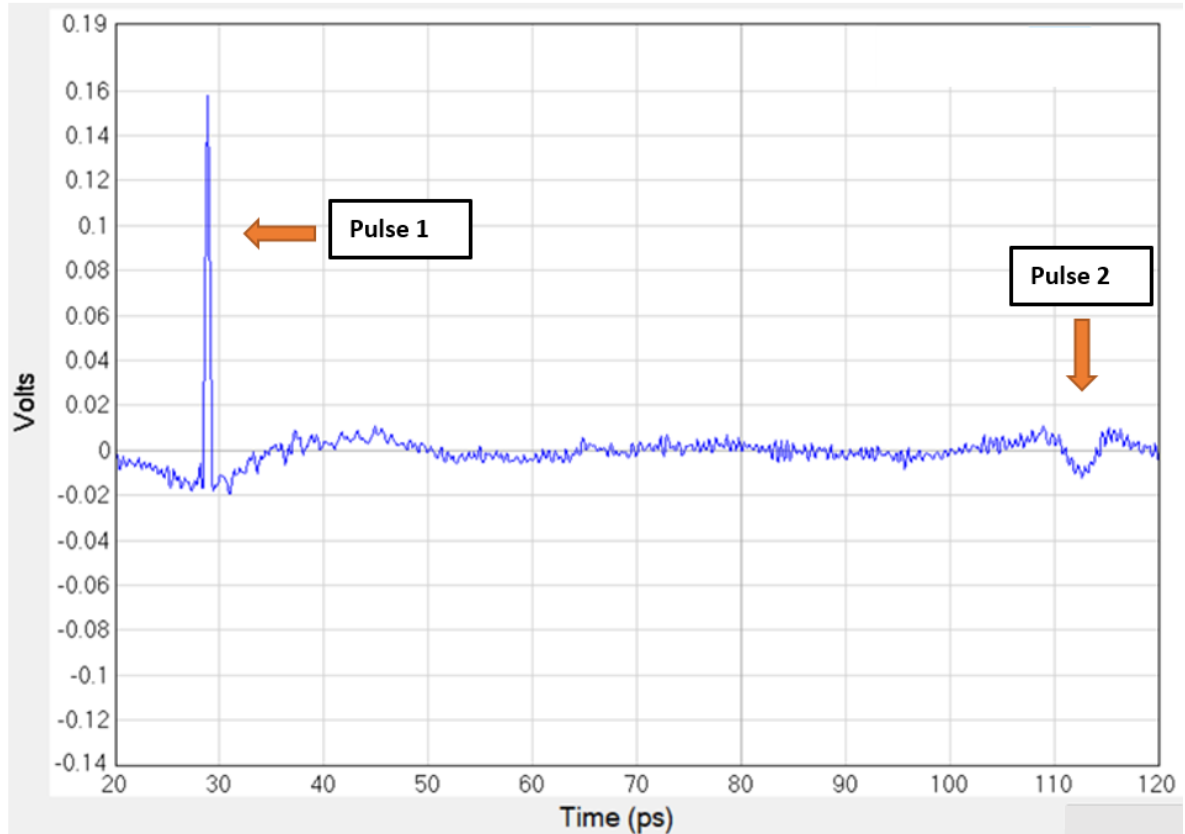


Figure 5.11 An example of a ‘11’ pixel in the clandestine tag as a deconvolved waveform.

For a pixel with an encoded plastic layer followed by an air gap layer (or a ‘10’ pixel), a pulse off the front surface is expected, followed by a 44-picosecond gap to the next pulse as it travels through two plastic layers. Next would be a 13-picosecond gap as it passes through the air layer back to plastic, and finally a 22-picosecond gap to reach the pulse from the back of the tag. This can be seen as a deconvolved wave in Figure 5.12.

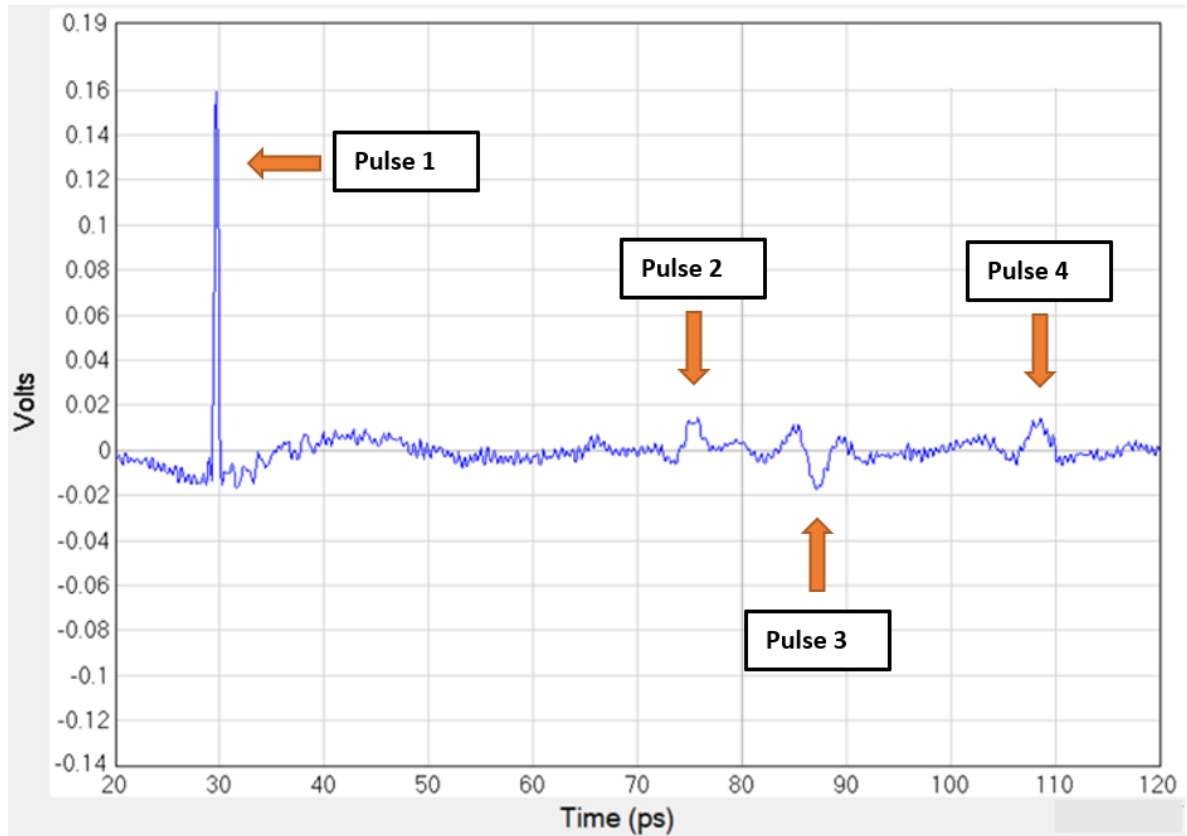


Figure 5.12 An example of a ‘10’ pixel in the clandestine tag as a deconvolved waveform.

For a pixel with two encoded air gaps in row (or a ‘00’ pixel), a pulse off the front surface is expected, followed by a 22-picosecond gap to the next pulse. A 26-picosecond gap to the next pulse is expected as it travels through two air layers back to plastic. Finally, a 22-picosecond gap brings it to the back surface for a final pulse.

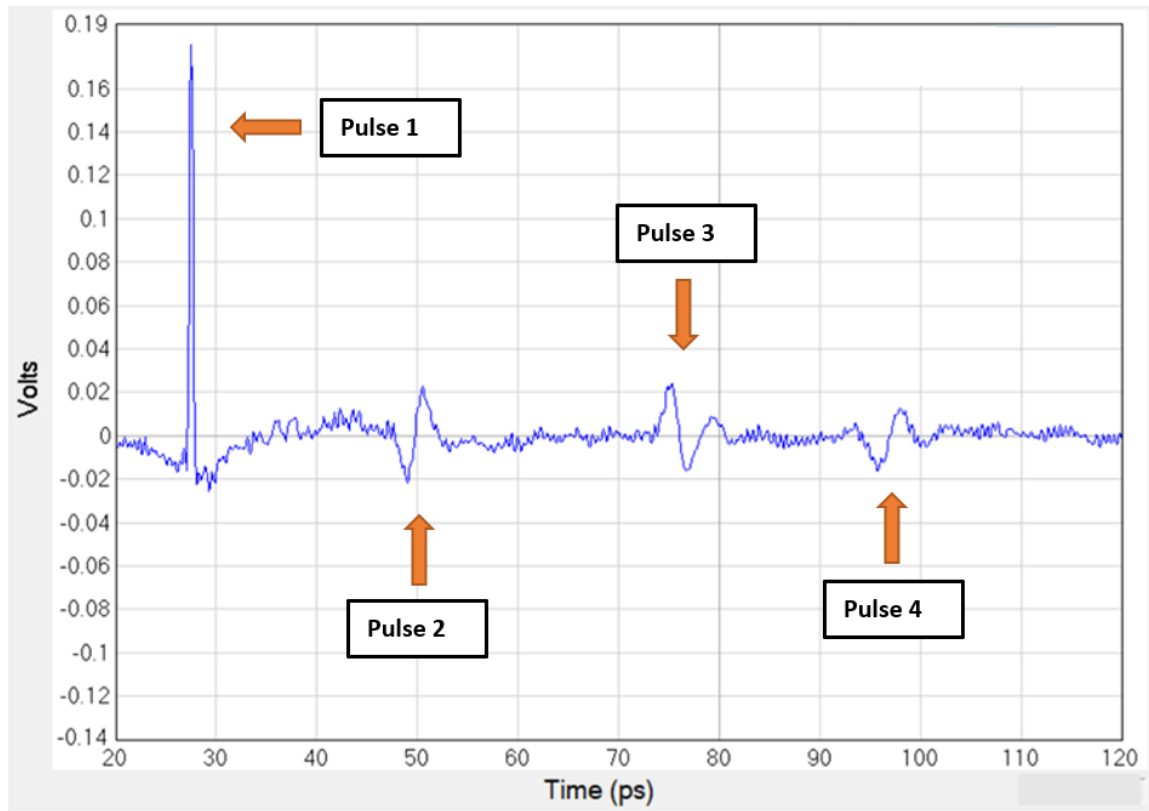


Figure 5.13 An example of a '00' pixel in the uncovered tag as a deconvolved waveform.

CHAPTER 6

ANALYSIS

6.1 Decoding Algorithm

A decoding algorithm was constructed to convert the data collected from the 3D QR code into its corresponding binary representation. The code was produced in MathWorks MATLAB.

The initial function of the code has the purpose of importing the picotd files that contain the data collected by the T-Ray 5000, representing the deconvolved THz time-domain waveforms manipulated by the structure of the 3D QR codes. The function reads and designates the data into an array with two columns, one for the time in picoseconds, and the other for the instantaneous THz electric field. The electric field value is recorded in units of volts corresponding to the output voltage of the electronic circuitry which detects the instantaneous electric field. This ensures that each time and its correlated voltage share the same row index. This function also discards the unnecessary header information contained in the files. This function can be found in Appendix A.

After the data for a pixel is imported, the decoding algorithm is employed, which can be found in Appendix B. It first searches for the maximum voltage within the waveform, which denotes the reflection from the front surface of the 3D QR code (as subsequent reflections will be attenuated). The time associated with the maximum voltage is logged, as this is used as a reference point for which the other time windows in the algorithm are determined.

The code then calculates how long it would theoretically take a THz pulse to travel through a layer of material based on its refractive coefficient and the thickness of the layer. This is determined for both PLA and air assuming 2 mm layers, but this could easily be altered to accommodate any material and thickness.

Given that the first layer of the structure is always plastic, a time window is constructed for which the first potential layer transition may occur. This is done by incorporating the time associated with the front surface reflection and the expected THz travel time through the first PLA layer. The time window was calculated to be between approximately 15 picoseconds and 25 picoseconds after the front surface pulse. The algorithm checks for a voltage above a certain threshold, which differentiates an interface pulse from noise. The threshold used was .014 volts, which represents approximately 10% of the voltage measured from the front surface reflection. This threshold was experimentally determined by assessing where pulses were expected and cutting off ‘pseudo-pulses’ created by random variation in the electric field. Based on the presence or absence of a pulse within this time window, a binary number is assigned.

The algorithm then splits into two branches based on which number was assigned. If a ‘0’ was assigned (signifying a pulse was found), this means that the second layer is air, and a new time window is constructed accordingly based on how long it will take the wave to reach the next potential layer interface. If a ‘1’ was assigned (signifying a pulse was not found), a time window is instead determined assuming the second layer is plastic. The algorithm once again searches for a pulse above a threshold in the new time window and assigns a second binary number depending on if it is found or not. The time intervals

and binary numbers assigned to each type of deconvolved waveform can be seen in Figures 6.1-6.4.

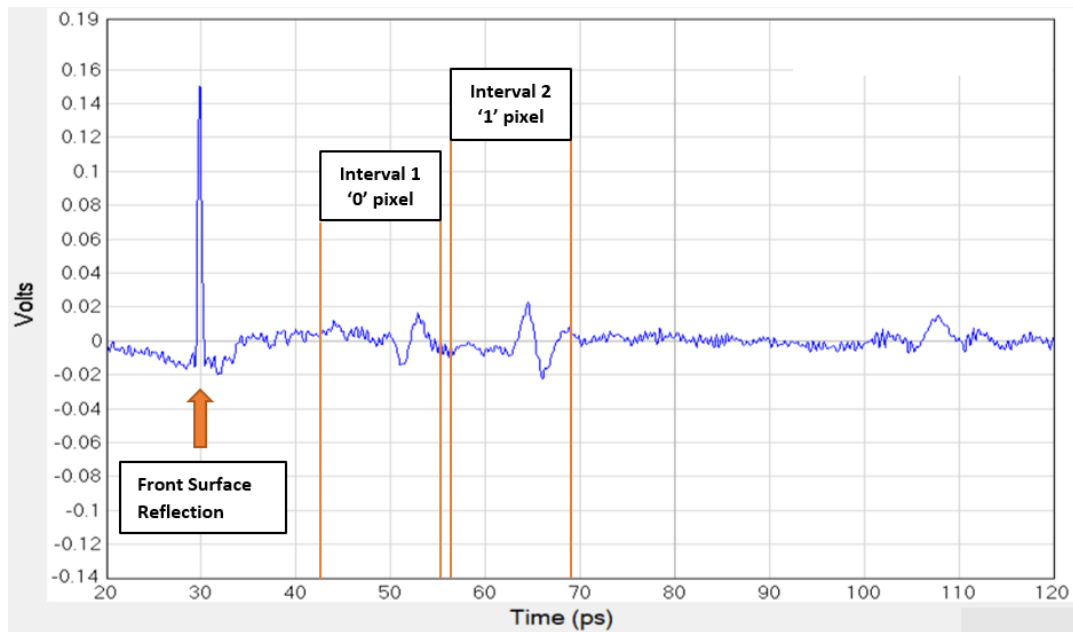


Figure 6.1 Time intervals and binary designation on '01' deconvolved waveform.

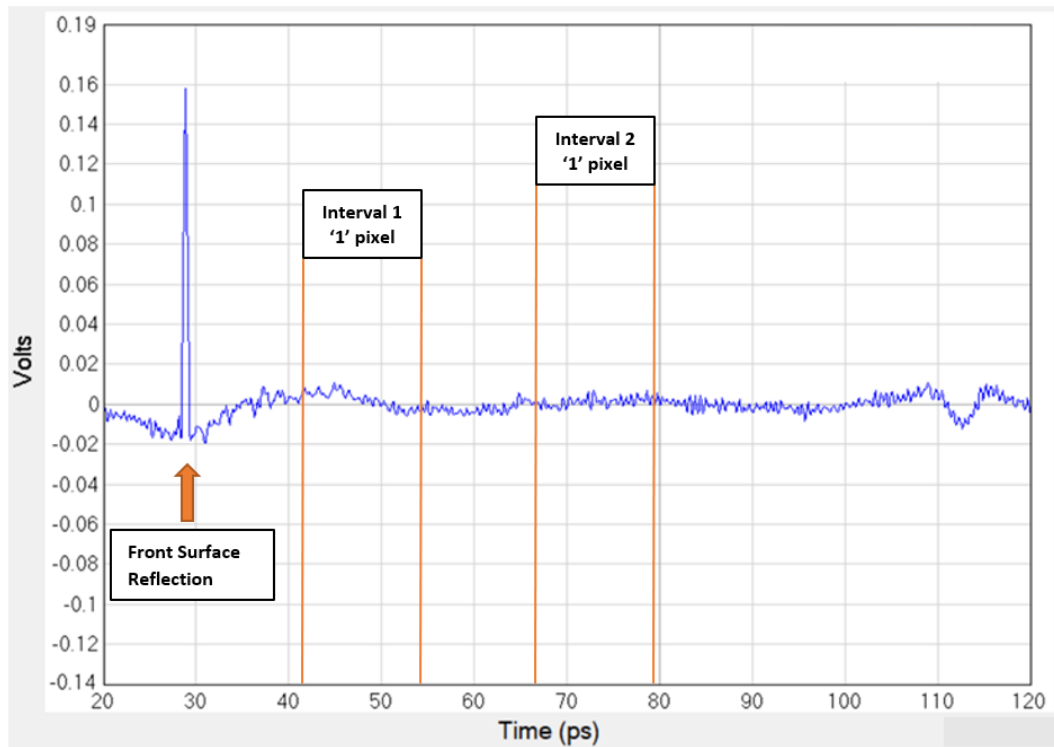


Figure 6.2 Time intervals and binary designation on '11' deconvolved waveform.

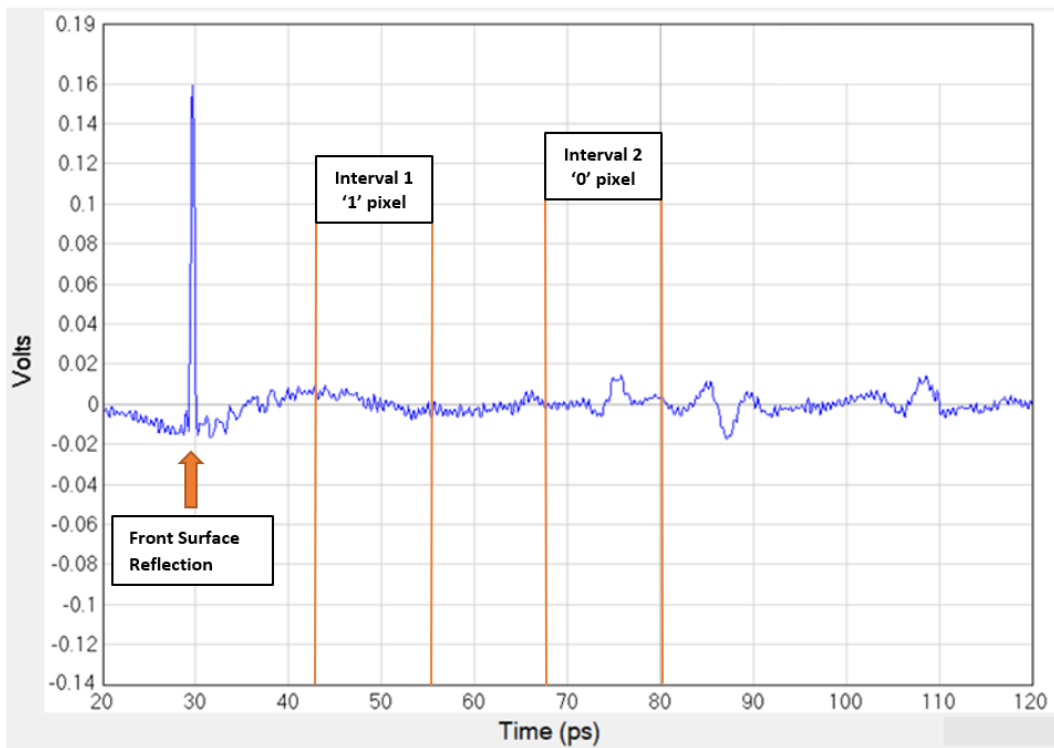


Figure 6.3 Time intervals and binary designation on '10' deconvolved waveform.

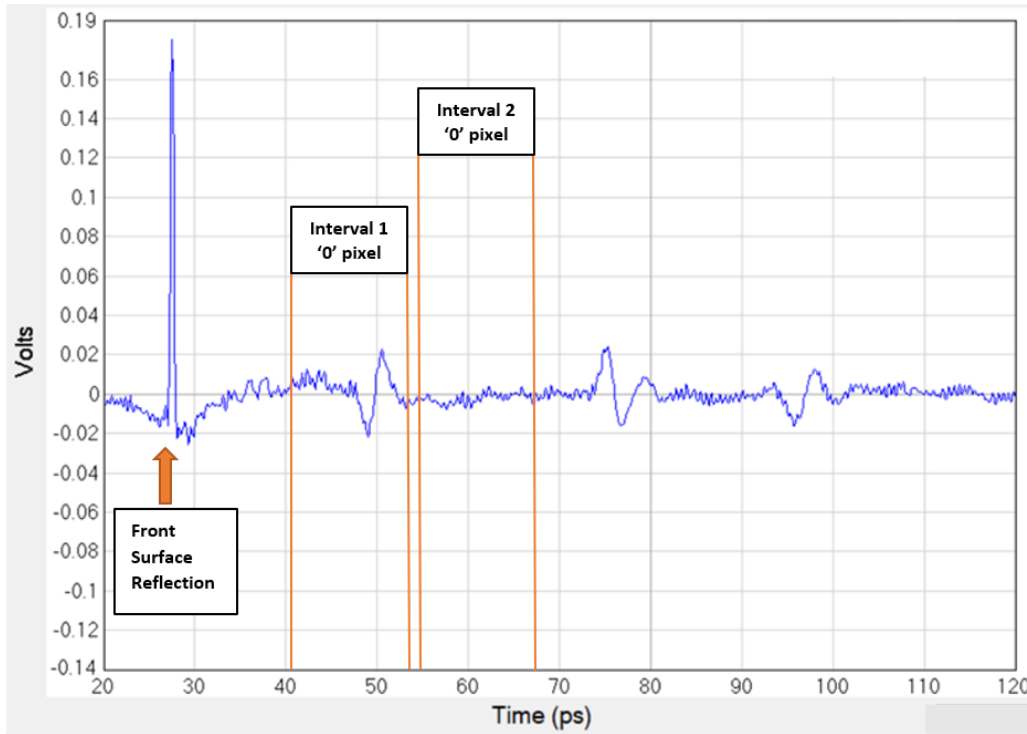


Figure 6.4 Time intervals and binary designation on ‘00’ deconvolved waveform.

The algorithm is built in a modular way so that it can easily be expanded to decode 3D QR codes with many more layers and interface changes. This idea is explored in more detail in Section 6.2.

In applying the algorithm to the data collected from the 3D QR code used in this study, each of the nine pixels was successfully decoded. The binary output matched the expected output as embedded in the physical geometry of the code’s structure, and a unique eighteen-digit code could be verified.

This process was also repeated for an identical copy of the clandestine code, printed separately from the original. While the deconvolved waveforms had the expected minor deviations from the original, the interface pulses were still found in their correct locations, and the copy was also decoded accurately.

6.2 QR Code Simulator

In order to test the decoding algorithm for 3D QR codes composed of more layers and/or different materials, a QR code simulator algorithm was produced in MATLAB. The script takes input in the form of a theoretical QR code design as defined in a Microsoft Excel spreadsheet. This includes the number of layers, the refractive index and absorption coefficient for the material in each layer, the ordering of the layers, and each layer's thickness. The algorithm uses the assumption that the real index of refraction and the attenuation coefficient for a material are independent of frequency, which for the simulated situation is approximately true. Fresnel coefficients are calculated using the equations found in Section 4.1 and are implemented in the algorithm. A real experimentally obtained reference file is also incorporated to help generate the data. The algorithm uses these parameters to simulate a THz wave interacting with the virtual 3D QR code, and outputs the resultant waveform. The QR simulator algorithm and EXCEL input file can be found in Appendix C.

Many QR codes were generated using this simulation and were successfully decoded using the algorithm used in the experimental portion of the study. This included when the indices of refraction and absorption coefficients were altered, when thicknesses of layers were changed, when the ordering of layers was rearranged, and when additional layers were introduced. A typical raw and deconvolved waveform are shown in Figure 6.5.

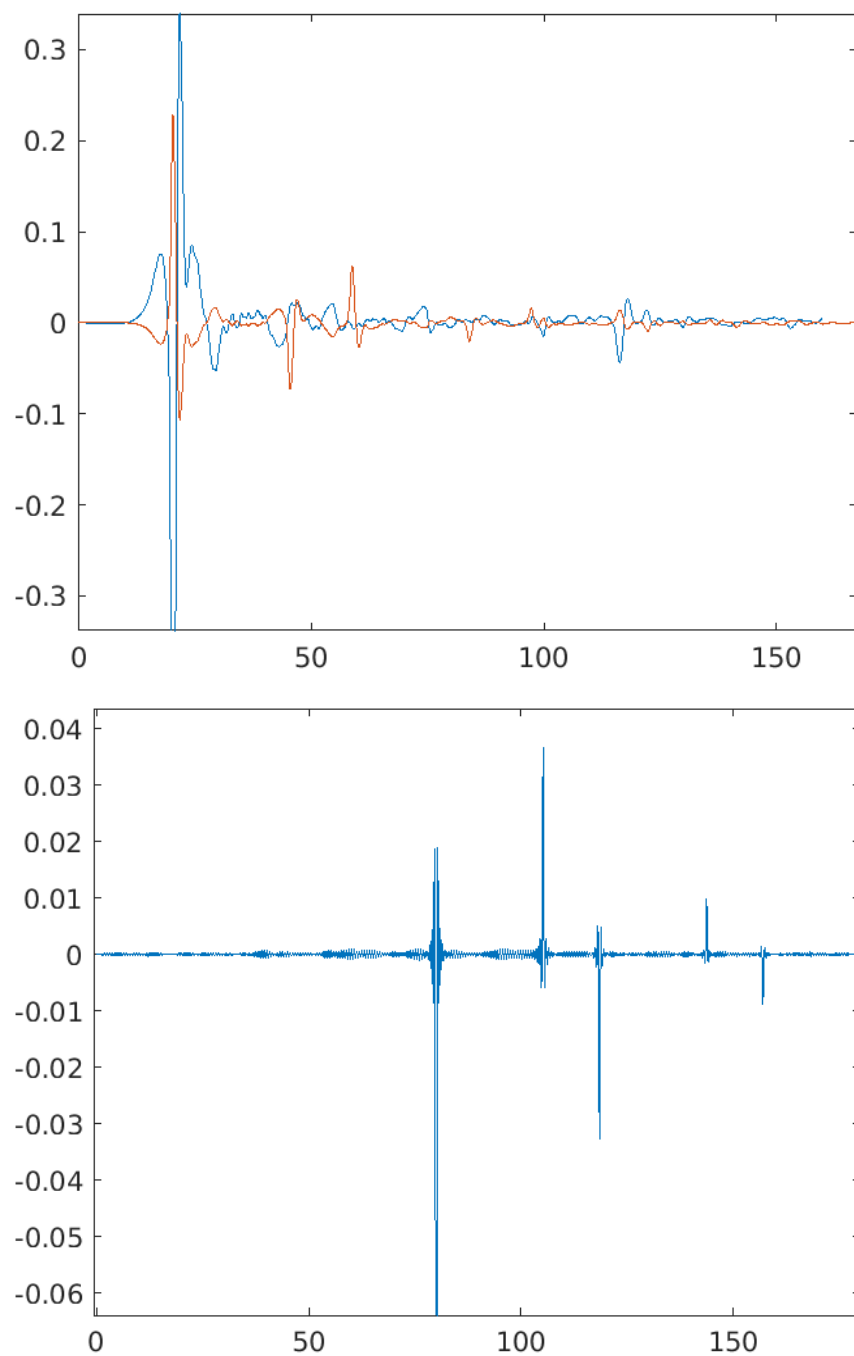


Figure 6.5 A typical raw (top) and deconvolved (bottom) waveform created by the QR code simulator. The first pulse extends to approximately -0.4 volts, but is truncated in order for other pulses to be visible.

A QR code was simulated that matched the geometry of the clandestine version discussed in Section 5.4. The simulation was consistent with experimental results in the

time domain, as the time delay between pulses in the deconvolved waves maintained the expected intervals. Consistency was not maintained between the amplitudes of the simulated and experimental deconvolved waveforms. For the simulated wave, the second reflection pulse reduced to approximately 33% of the amplitude of the initial front reflection. At best, the second pulse dropped to approximately 20% of the initial pulse in the experimental version, though it was often even smaller. This is most likely due to the assumption made in the simulator that attenuation is independent of frequency, which is not fully true. This results in simulator pulses being unrealistically sharp, letting it maintain higher amplitudes, while experimental pulses are temporally broader. A simulated ‘01’ pixel can be seen in Figure 6.6, which can be compared to its experimental counterpart in Figure 6.1.

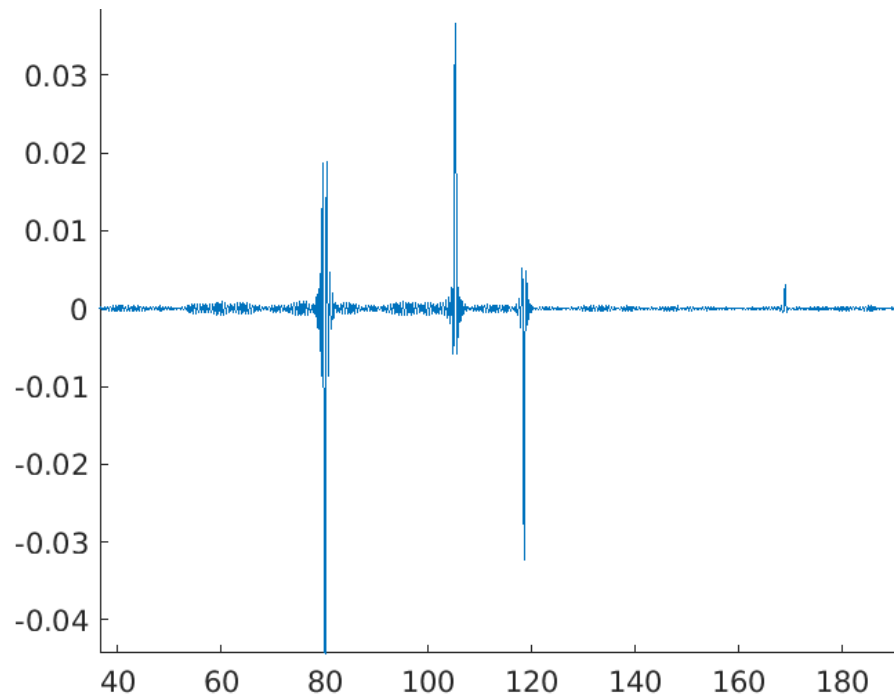


Figure 6.6 A deconvolved simulated ‘10’ pixel for a four-layer structure.

Limitations were introduced when either too many layers were introduced, or when the thickness of individual layers were too small. Using the index of refraction and absorption coefficient or PLA in Table 4.1, a seven-layer code was produced alternating plastic and air layers of 2 mm thickness. As the simulated wave passed through each PLA layer, it was attenuated significantly. While the sample could be decoded correctly, the algorithm threshold had to be lowered to a smaller value (0.009). This may cause difficulties in an environment with experimentally generated noise, as noise amplitude commonly exceeded this value earlier in this study. The deconvolved form of this wave is depicted in Figure 6.7. Even with threshold changes, any layers past the seventh could not be decoded accurately, as the pulses fully blended into noise. In addition to this, a six-layer pixel was simulated containing only PLA layers, in which the final back surface reflection could still be decoded accurately. Any layers beyond this also blended into noise, meaning that at most a 3D QR code can have a depth of 12 mm before the attenuation becomes too great.

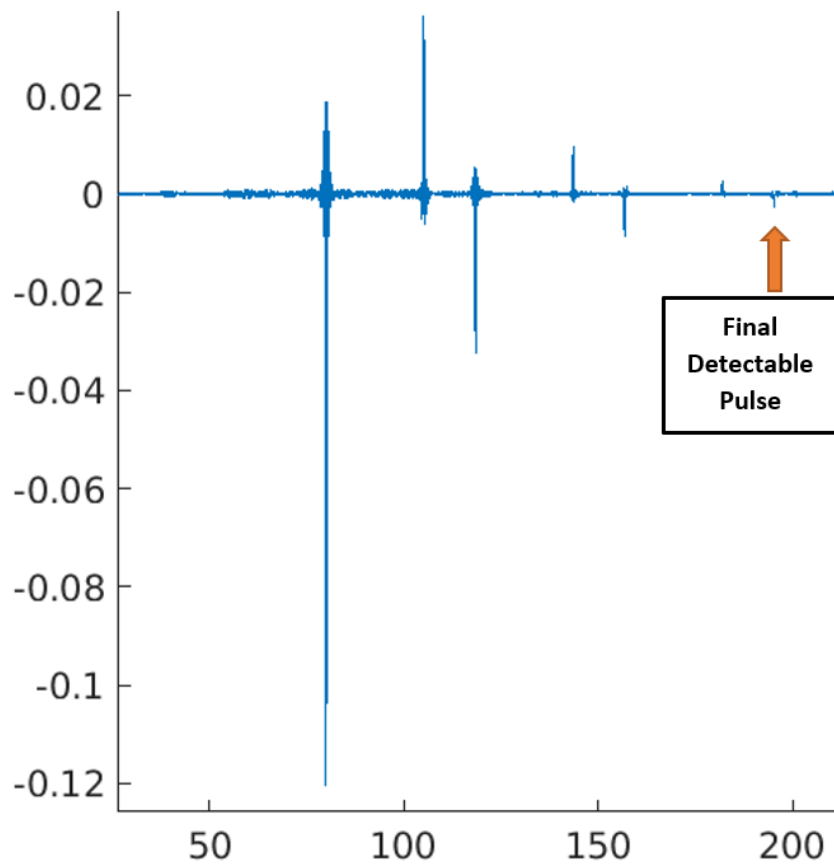


Figure 6.7 Example of simulated QR code attenuated to decoding limit.

A similar five-layer structure was simulated using the same parameters as the previous QR code, but the thickness of each layer was reduced to .02 mm. At this point, the widths of the pulses were overlapping and interfering. While pulses can be seen, they are clearly unreliable as they increase in amplitude throughout the structure when it is expected that they should decrease. In an experimental situation, decoding such a structure would be even more problematic, as deconvolved pulse widths had some random variation. This deconvolved wave is depicted in Figure 6.8. Wave overlap could be avoided when the thickness of layers was shifted to approximately 0.05 mm.

Studies have been conducted to develop methods for resolving overlap in the THz time domain, namely in investigating multilayer paint structures. These paint layers can be on the order of .018 mm, and techniques involving multiple regression analysis using the least-square fitting process are required to deal with overlap interference [Yasuda et al. 2007]. Considerations such as the absorption and dispersion of materials, as well as the etalon effect, have also since been integrated into these methods [Su et al. 2014]. Similar approaches may be applicable in decoding QR codes with thin layers, though these means will not be explored further in this thesis.

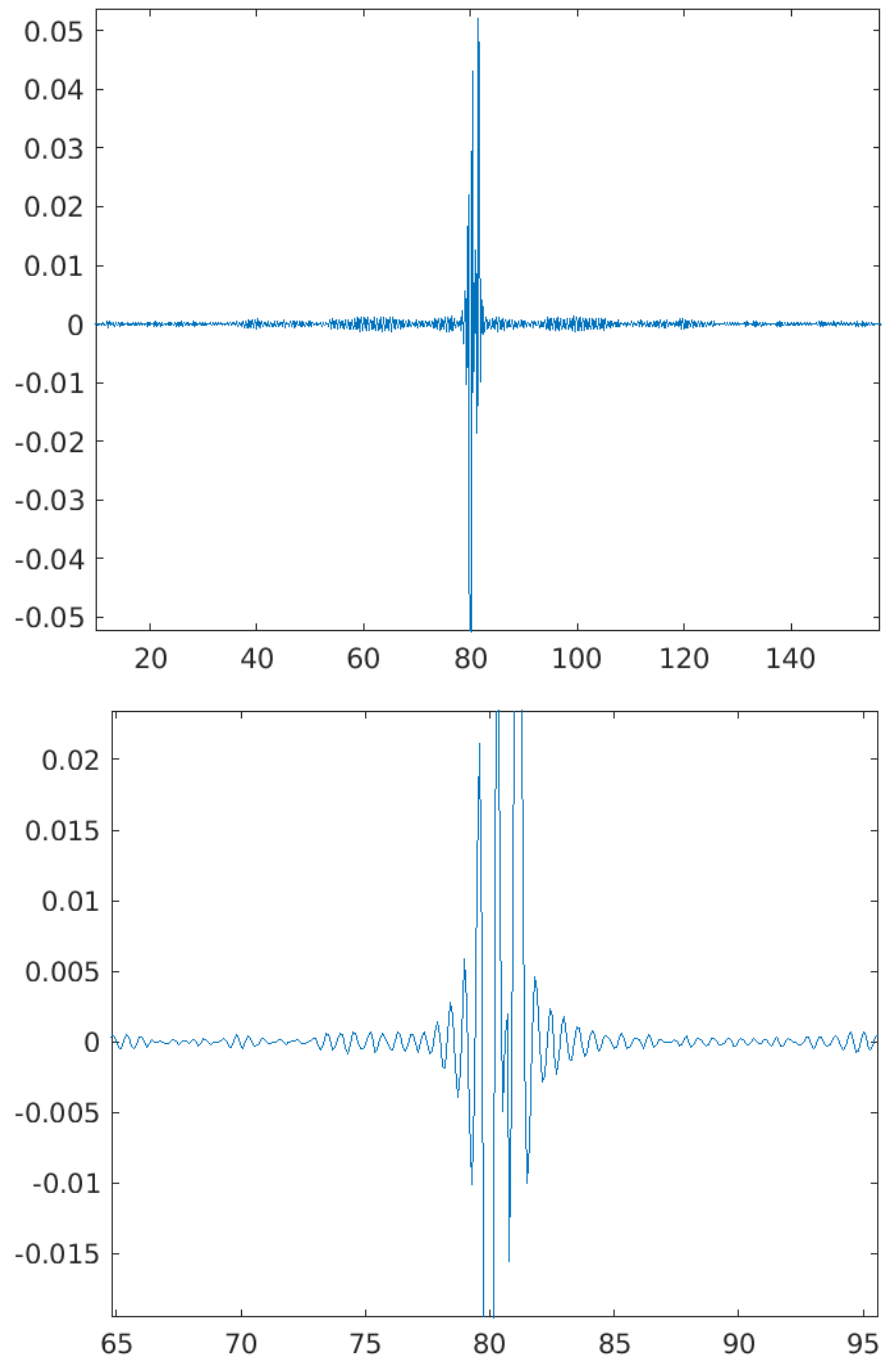


Figure 6.8 Example of simulated QR code with thin layers leading to waveform overlap viewed with a wide (top) and narrow (bottom) time axis.

CHAPTER 7

CONCLUSION

7.1 Results

Through this study, it was shown that it is possible to produce a 3D QR code through additive manufacturing, noninvasively determine its internal geometry using THz radiation, and output a unique code using a decoding algorithm. The four-layer clandestine sample in this study was constructed in a single print, and all nine pixels were decoded accurately, resulting in an eighteen-digit binary code. Furthermore, it was displayed that tags consisting of more layers or composed of different materials could be theoretically fruitful as well, as the decoding algorithm was applied to simulated 3D QR codes. The proof of concept this study set out to explore was fulfilled.

Limitations in the design of a 3D QR code were also revealed through both the experimental and simulated portions of the study. For accurate decoding, it was determined that the lateral size for pixels in a QR code should not be designed below 4.8 mm for a 3-inch lens. In using PLA, each layer should not be below .05 mm in thickness due to pulse overlap, and the overall structure should not exceed 1.2 cm to avoid significant attenuation. It was determined that the attenuation limits the tag's total depth rather than the Rayleigh range, which was calculated at a much larger 7 cm. Given these parameters, the maximum number of stored bits in a single pixel is approximately 240. A 9-pixel structure would correspond to a 14.5 mm by 14.5 mm by 12 mm structure and contain approximately 2,160 bits.

7.2 Future Research/Applications

The 3D QR codes produced in this study could act as a basis to many potential research and application opportunities. As technology centered around THz radiation progresses, many of the difficulties mentioned in this study can be circumvented, and convenience in using such a tag would be more plausible. Future experiments could be concerned with expanding on the number of layers or pixels in a structure. The ability to identify and scan pixels may also be automated, as well as data being seamlessly transferred into a decoding algorithm.

Future research could also focus on the material choice of the tags. While PLA and air were used in this study, recent developments in thermoplastics embedded with ceramics could remove the need for an air gap entirely. Fused Deposition Modeling filaments comprised of PLA and ABS plastics embedded with ceramic particulates are currently available, and results in a material with a refractive index much larger than the plastic itself. By varying the amount of ceramic which is mixed into the plastic, one may increase the real permittivity to the 4 or larger. When paired with their non-ceramic counterpart, these plastics could offer a similar index differential to that found in this study (approximately 0.9) without the need for air gaps.

A study may also be conducted exploring the angle of incidence of THz radiation on a 3D QR code. As mentioned in Section 2.1, a study by M. Bernier et al. featured the angle tolerance of a similar type of tag, and decoding was shown to be disrupted for even small changes in the angle. Since this would limit the type of applications possible for a tag, this may be an interesting parameter to experiment with. Since the tags featured in this study were measured with reflection, they would likely have a greater tolerance for

changes in the incident angle. For instance, for a 15-degree incident angle would only result in an approximately 1 ps shift in the time domain for a THz pulse. Since the decoding algorithm uses time windows on the order of 10 ps, it can be expected that the tag would still be properly decoded.

There are numerous places where such a tag may be useful in application. As additive manufacturing continues to gain popularity, being able to easily and instantly incorporate a tag in creations for inventory purposes is helpful. Such tags can also be considered environmentally friendly, as no additional packaging may be required. The information is also secure, as the internal code can only be read out noninvasively through THz radiation, which may have military or personal encryption purposes. These are just a few suggestions for a seemingly limitless amount of potential uses for such a tag.

APPENDIX A

IMPORT FUNCTION

The following function has the purpose of importing the picotd files that contain the data collected by the T-Ray 5000, representing the deconvolved THz time-domain waveforms manipulated by the structure of the 3D QR codes.

```
function [time,voltage] = importPicoTDfile(filename)
%IMPORTFILE Import numeric data from a text file as column vectors.
% [TIME,VOLTAGE] = importPicoTDfile(FILENAME) Reads data from picotd text
file
% FILENAME. The information in the header for the file is ignored. The
corresponding
% time (units of picoseconds) and THz voltage for time-domain waveform is
returned.

%% Initialize variables.
delimiter = '\t';
startRow = 5;

%% Format for each line of text:
% column1: double (%f)
% column2: double (%f)
% For more information, see the TEXTSCAN documentation.
formatSpec = '%f%f*s*s*s*s*s*s*s*s[\n\r]';

%% Open the text file.
fileID = fopen(filename,'r');

%% Read columns of data according to the format.
% This call is based on the structure of the file used to generate this
% code. If an error occurs for a different file, try regenerating the code
% from the Import Tool.
textscan(fileID, '%[\n\r]', startRow-1, 'WhiteSpace', '', 'ReturnOnError',
false, 'EndOfLine', '\r\n');
dataArray = textscan(fileID, formatSpec, 'Delimiter', delimiter, 'TextType',
'string', 'ReturnOnError', false);

%% Close the text file.
fclose(fileID);

%% Allocate imported array to column variable names
time = dataArray{:, 1};
voltage = dataArray{:, 2};

%% Clear temporary variables
clearvars filename delimiter startRow formatSpec fileID dataArray ans;
```

APPENDIX B

DECODING ALGORITHM

The following function is used to convert the imported deconvolved waveform data from a 3D QR code into its corresponding binary code representation based on its internal geometry.

```
% Imports time and voltage from picotd file as column vectors.
[time,voltage] = importPicoTDfile('1Deconvolved.picotd');

% Determines max voltage of waveform, its index, and associated time.
% This represents the amplitude and time of the
% pulse reflected from front surface of sample.
[maxvolt,I] = max(voltage);
front = time(I,1);

% Initializes threshold, above which is measured as a boundary transition.
thresh = .014;

% Initializes speed of light, refractive indices, and layer thickness
lightspeed=299792458;

plaref=1.89;
airref=1.0003;

layerthick=.002;

% Determines time intervals expected for propagation through plastic
% and air layers
plaint = round(2*((layerthick/(lightspeed/plaref))*10^12));
airint = round(2*((layerthick/(lightspeed/airref))*10^12));

% Determines indices for the beginning and end of time interval
% where first internal boundary transition may occur as a function
% of the front surface time.
timestart=round((front+airint)/.1);
timeend=round((front+plaint)/.1);

% Initializes index intervals expected from air and plastic layers.
airind=(airint/.1);
plaind=(plaint/.1);

% Checks if a boundary transfer occurs at first potential transition
% interval, and assigns/displays corresponding binary number.
if (max(abs(voltage(timestart:timeend)))) > thresh
    x=0;
    disp(x)
```

```

else x=1;
    disp(x)
end

% Establishes a new transition interval based on previous binary
% number, checks for boundary transition in new interval, and
% assigns/displays second binary number.

if x==0

    timestart=timestart+airind;
    timeend=timeend+airind;

    if (max(abs(voltage(timestart:timeend)))) > thresh
        x=1;
        disp(x)
    else
        x=0;
        disp(x)
    end
else

    timestart=timestart+plairind;
    timeend=timeend+plairind;

    if (max(abs(voltage(timestart:timeend)))) > thresh
        x=0;
        disp(x)
    else
        x=1;
        disp(x)
    end
end

% The final section of code can be reiterated for additional
% encoded layers to generate more robust binary codes. This is
% utilized in decoding the QR Code simulator data.

```

APPENDIX C

QR CODE SIMULATOR

The EXCEL file and program are used together to generate simulated 3D QR codes.

1	% input file to run simulation of QR-CODEs					
2	version	1	StartDataRow	5	EndDataRow	9
3	parameters to determine attenuation coefficient					
4	thickness(mm)	n real	alpha0 (mm ⁻¹)	alpha1 (mm ⁻¹ /THz)	alpha2 (mm ⁻¹ /THz ²)	comments
5	2	1.88	0.28	0	0	PLA
6	2	1	0	0	0	air
7	2	1.88	0.28	0	0	PLA
8	2	1	0	0	0	air
9	2	1.88	0.28	0	0	PLA
10						

Figure C.1 Example of parameters defined in EXCEL file used in producing simulated 3D QR codes.

C.2 QR Code Simulator Main Program

```
% QR Code simulator main program for
% simple solution in TIME DOMAIN.
%
% read in design of QR Code
c=299792458; % speed of light in m/s
FilterSpec='/MATLAB Drive/*.xls'
prompt='What is the QR-CODE excel design File Name?'
[RefName,RPathName,FilterIndex] = uigetfile(FilterSpec,prompt);
FName=[RPathName,RefName]

% read in version of table format
opts = spreadsheetImportOptions("NumVariables", 2);
% Specify sheet and range
opts.Sheet = "Sheet1";
opts.DataRange = "A2:B2";
opts.VariableTypes = ["string", "double"];
% Import the data
QRCODE_table_version = readtable(FName, opts, "UseExcel", false);
disp(QRCODE_table_version)
%
% read starting row of data
opts = spreadsheetImportOptions("NumVariables", 1);
opts.VariableTypes = "double";
opts.DataRange = "D2:D2";
% Import the data
DunnQRCODE = readtable("/MATLAB Drive/Dunn_QRCODE3.xlsx", opts, "UseExcel",
false);
StartRow = table2array(DunnQRCODE);
% read ending row of data
opts.DataRange = "F2:F2";
opts.VariableTypes = "double";
% Import the data
```

```

DunnQRCODE = readtable("/MATLAB Drive/Dunn_QRCODE3.xlsx", opts, "UseExcel",
false);
EndRow = table2array(DunnQRCODE);
numlay=EndRow-StartRow+1; % number of layers in QR-CODE
% Specify column names and types
opts = spreadsheetImportOptions("NumVariables", 3);
opts.VariableNames = ["Thickness", "nReal", "a0"];
opts.VariableTypes = ["double", "double", "double"];
str=sprintf('A%d:C%d',StartRow,EndRow);
opts.DataRange = str;

% Import the data
tbl = readtable("/MATLAB Drive/Dunn_QRCODE3.xlsx", opts, "UseExcel", false);

%% Convert to output type
Thickness = tbl.Thickness;
nReal = tbl.nReal;
a0 = tbl.a0;

%% Clear temporary variables
clear opts tbl str StartRow EndRow

%
% read in reference pulse waveform
FilterSpec='/MATLAB Drive/*.picotd';
prompt='What is the Reference File Name?'
[RefName,RPathName,FilterIndex] = uigetfile(FilterSpec,prompt);
FName=[RPathName,RefName]
[t1,Einc] = importPicoTDfile(FName); % Reference time and reference voltage
data
%Rescale time from pico seconds to seconds
DeltaT=0.1e-12; % 0.1 ps time interval
itime=[1:1600*2]; %define OUTPUT Efield array to be 2 times time duration of
THz pulse.
Eout(itime)=0; % initialize output waveform.
% time index of reference waveform is from 1 to 1600
n0=1; % refractive index of air
Einc=Einc-mean(Einc(1:20)); % subtract off background for reference waveform
% Einc=-Einc; % use this line if reference waveform from reflection form
mirror.
%
% reflected wave from air-front surface
iTstart=0; % starting time of reflected pulse
for j=1:1600
    Eout(j+iTstart)=Eout(j+iTstart)+Einc(j)*reflCoeff(n0,nReal(1));
end
TransTemp=transCoeff(n0,nReal(1))*transCoeff(nReal(1),n0)*exp(-
2*a0(1)*Thickness(1)); % transmission coefficient from air-front surface,
through material,
    % back through material and across boundary
%
for i=2:numlay% now calculate reflected wave from each boundary
    iTstart=iTstart+round(2*Thickness(i)*1e-3*nReal(i-1)/c/DeltaT) ; %
calculate index of starting time of reflected pulse

```

```

    Etemp=Einc*TransTemp*reflCoeff(nReal(i-1),nReal(i)); % reflected pulse
    from this boundary
    for j=1:1600
        Eout(j+iTstart)=Eout(j+iTstart)+Etemp(j);% add pulse to pulse train
    end
    TransTemp=TransTemp*transCoeff(nReal(i-
1),nReal(i))*transCoeff(nReal(i),nReal(i-1))*exp(-2*a0(i)*Thickness(i)); %
update transmission coefficient for next iteration
end
% reflected wave from back surface-air boundary
iTstart=iTstart+round(2*Thickness(numlay)*1e-3*nReal(numlay)/c/DeltaT) ; %
calculate index of starting time of reflected pulse
for j=1:1600

Eout(j+iTstart)=Eout(j+iTstart)+Einc(j)*TransTemp*reflCoeff(nReal(numlay),n0)*
exp(-2*a0(numlay)*Thickness(numlay)); % add pulse to pulse train
end
%
% create time axis for plots
timeQR=[0:0.1:(160*2-0.1)];
plot(t1,Einc,timeQR,Eout) % plot incident and reflected waveform
%
DeConv=deconvreg(Eout,transpose(Einc)); % deconvolve output waveform
figure; % simple deconvolution to get deconvolved peaks
plot(timeQR,DeConv)
%
function refl = reflCoeff(n1,n2)
% Fresnel reflection coefficient
% Input parameters
% n1 - index of refraction on incident side
% n2 - index of refraction on transmitted side
%
refl=(n1-n2)/(n2+n1);
end
%
function trans = transCoeff(n1,n2)
% Fresnel transmission coefficient
% Input parameters
% n1 - index of refraction on incident side
% n2 - index of refraction on transmitted side
%
trans=1+(n1-n2)/(n2+n1);
end

```

REFERENCES

- Bernier, M., Garet, F., Perret, E., Duvillaret, L., & Tedjini, S. (2011). Terahertz encoding approach for secured chipless radio frequency identification. *Applied optics*, 50(23), 4648-4655.
- Brillouin, L. (1953). *Wave propagation in periodic structures: Electric filters and crystal lattices*. New York: Dover Publications.
- Busch, S. F., Weidenbach, M., Fey, M., Schäfer, F., Probst, T., & Koch, M. (2014). Optical properties of 3D printable plastics in the THz regime and their application for 3D printed THz optics. *Journal of infrared, millimeter, and Terahertz waves*, 35(12), 993-997.
- Chan, W. L., Deibel, J., & Mittleman, D. M. (2007). Imaging with Terahertz radiation. *Reports on Progress in Physics*.
- Dong, J., Jackson J., Melis M., Giovanacci D., Walker G., Locquet A., Bowen J., & Citrin D., (2016) Terahertz frequency-wavelet domain deconvolution for stratigraphic and subsurface investigation of art painting. *Opt. Express* 24, 26972-26985 .
- Kato, H., & Tan, K. (2007). Pervasive 2d barcodes for camera phone applications. *IEEE Pervasive Computing* 6–85.
- Mølster, K. M. (2017). *THz time domain spectroscopy of materials in reflection and transmission* (Master's thesis, NTNU).
- Redo-Sanchez A. (2012). *The Terahertz Wave EBook*. Zomega Terahertz Corporation. Apple Books. 6-9.

- Saleh, Bahaa E. A., & Malvin C. Teich. (1991). *Fundamentals of Photonics*. New York: Wiley.
- Siegel, P H (2003). THz technology: An overview. *International Journal of High Speed Electronics and Systems*, 13(2), 351–394
- Smyth, Clifford. (2017) *Functional Design for 3D Printing*. 3rd ed., Self-Published.
- Su K., Shen Y., & Zeitler J. (2014), Terahertz sensor for non-contact thickness and quality measurement of automobile paints of varying complexity. *IEEE Trans. THz Sci. Technol.*, vol. 4, no. 4, pp. 432–439
- Subramanian, V., Frechet, J., Chang, P., Huang, D., Lee, J., Molesa, S., Murphy, A., Redinger, D., & Volkman, S. (2005). Progress toward development of all-printed RFID tags: Materials, processes, and devices. *Proc. IEEE*, 1330–1338.
- Willis, K. D., & Wilson, A. D. (2013). InfraStructs: fabricating information inside physical objects for imaging in the Terahertz region. *ACM Transactions on Graphics (TOG)*, 32(4), 138.
- Yang, Y., & Fathy, A. (2005). See-through-wall imaging using ultra wideband short-pulse radar system. *In Proc. Antennas and Propagation Soc. Int. Symp.*, vol. 3B, IEEE, 334–337.
- Yasuda T., Iwata T., Araki T., & Yasui T. (2007). Improvement of minimum paint film thickness for THz paint meters by multiple-regression analysis. *Appl. Opt.*, vol. 46, pp. 7518–7526.